Master Thesis

Majorana bound states in spatially inhomogeneous nanowires

Author:
Johan Ekström

Supervisor:
Assoc. Prof. Martin Leijnse

Division of Solid State Physics
Faculty of Engineering

November 2016

LUNDS
UNIVERSITET

Abstract

Majorana bound states are in condensed matter physics quasiparticle excitations which can be found in so-called topological superconductors. They have lately received much attention since they have been predicted to be partly immune to decoherence and therefore suitable for quantum computation. A nanowire with strong spin orbit coupling and proximity induced superconductivity that is subject to a magnetic field has been shown to host a pair of Majorana bound states living on the opposite ends of the nanowire. One bit of quantum information (a qubit) can be stored in such a pair of Majorana bound states. The quantum information is then protected from decoherence as long as the Majorana bound states are well separated, such that their wave functions do not overlap. In this work we explore the effect of introducing potential barriers in the nanowire. It is shown that for certain parameter settings of the barriers the overlap between the Majorana bound states can be reduced. Furthermore, disorder in the potential is studied. The effect of the disorder is also shown to depend on the parameter settings of the barriers. Finally it is shown that a rotating magnetic field can amplify the spin-orbit coupling in a nanowire. Increasing the spin-orbit coupling results in a decrease in the overlap.

Acknowledgement

I would like to thank my supervisor Martin Leijnse for both giving me the opportunity to work on this project and also for the support and guidance I have received. I am also grateful to you for helping me out with matters not concerning my thesis. I would also like to thank Michael Hell and Florinda Viñas for discussing and helping me out with various matters.

Contents

Chapter 1

Introduction

1.1 Background

The idea of Majorana bound states stems from the Majorana fermions in particle physics. In particle physics a Majorana fermion is a particle that is its own anti-particle. The Majorana fermion was proposed in 1937 by Ettore Majorana, thereby its name, when he found that by making a clever modification to the Dirac equation it only involves real numbers [1]. It is not certain if the particle exists as an elementary particle but in condensed matter physics they are likely to exist as quasiparticle excitations of the many-body groundstate, which we call Majorana bound state (MBS) [2, 3]. MBSs are exotic states of matter that exist in so called topological superconductors and have lately received much attention due to their potential usefulness as building blocks for a quantum computer [4].

There are suggestions for many different systems hosting MBSs. Examples of these are the fractional quantum Hall states at filling factor $\nu = 5/2$, p-wave superconductors, heterostructures of topological insulators and superconductors, and spin-orbit coupled ferromagnetic Josephson junctions [5, 6]. Another example is nanowires with strong spin-orbit coupling in proximity to an s-wave superconductor which hosts a MBS on each end of the nanowire. The MBSs are zero-mode excitations that are well separated from the bulk states by an energy-gap. A MBS can furthermore be thought of as a half fermion. This means that a fermoinic state can be written as a superposition of two MBSs. This is normally just a mathematical operation without any physical consequences when the states are localized close to each other and when there is a significant overlap between the wave functions.

In nanowires MBSs on the opposite ends can in special cases, which is shown later, together form a "special" fermonic state. Since the MBSs live on opposite ends of the wire these will form a fermionic state that is highly delocalized. When e.g. a quantum state interacts with an environment, the environment may cause *decoherence*. This means that quantum state and the environment become entangled. Due to the entanglement information about the quantum state is lost [7]. However, since the highly delocalized fermionic state cannot be changed by perturbations only affecting one of its Majorana constituents, it is protected against most types of decoherence. Due to this property the MBSs are expected to give the possibility of low decoherence quantum computation[2, 4]. This property is however only kept as long as the MBSs are well separated and do not overlap.

One way to possibly realize a quantum computer is to build networks using nanowires hosting MBSs [8]. When one wants to build networks and make connections between the nanowires, the

nanowires are going to be shorter. This leads to that the MBSs in the nanowire will possibly overlap (depending on the length of the nanowire) and the possibility of low decoherence might be lost. This problem is what is going to be addressed in this project.

1.2 Thesis objectives

In this thesis we investigate MBSs in nanowires with spin-orbit coupling and proximity induced superconductivity, more specifically we want to try if it is possible to modulate the potential in the nanowire such that the overlap between the MBSs is reduced. The potential can be modulated by having gate-electrodes inducing a local potential shift in the nanowire. Another way to modulate the potential in a nanowire is by growing a nanowire with two different types of materials that has different badgap. The potential difference is then set by the offset in the conduction band between the two materials.

Due to the required stability of the MBSs in for example quantum computing, the effects of disorder is studied. We also investigate if a nanowire with modulation of the potential is affected differently by disorder compared to the homogeneous nanowire. Furthermore we investigate nanowires with and without spin-orbit coupling subjected to a helical magnetic field. The goal of this is the same as for the modulation of the potential; to try to find out if it is possible to reduce the overlap between the MBSs in the nanowire.

1.3 Superconductivity

To realize MBSs in nanowires, one ingredient is as mentioned proximity induced superconductivity. Proximity induced means that a superconductor induces so called Cooper-pairs into, in this case, the nanowire which makes it superconducting. Due to this we give a short introduction to superconductivity.

When certain materials are cooled below a critical temperature the material experience a phase transition and enters a superconducting phase. In the superconducting phase the electrical resistance is zero. This phenomena was first discovered in 1911 by Kamerlingh-Onnes when he observed the disappearance of the electrical resistance when cooling different metals below the critical temperature, T_c, of the investigated material. The explanation of the phase transition for conventional superconductors (superconductor with pairing of electrons with different spin, also denoted s-wave superconductor) was given by Bardeen, Cooper and Schriffer (BCS) in the BCS theory [9]. The BCS theory originated from an observation made by Cooper. He considered the problem of a pair of electrons interacting above a non-interacting Fermi sea of electrons and where the only interaction between the free electrons and the Fermi sea is via the Pauli exclusion principle. From this observation it was found that the electrons can form a bound state, a Cooper pair, if the sum of the total interaction is attractive. The reason for the attractive interaction is due to electron-phonon interactions. It can furthermore be shown that the interaction is strongest when the wave vector and the spin of the electrons are opposite. Due to this it is only necessary to consider Cooper pairs with ($\mathbf{k}\uparrow$ and $-\mathbf{k}\downarrow$) [10]. This effective positive interaction at the surface of the Fermi-sea renders it unstable and leads to formation of more Cooper-pairs. This goes on until equilibrium is reached. Due to this, BCS suggested that the wave function for the superconducting ground state could be written as superposition of states each with an integer number of Cooper pairs [11]. The ground state is written

$$|\psi_{BCS}\rangle = \prod_{\mathbf{k}} (u_{\mathbf{k}} + v_{\mathbf{k}} c^{\dagger}_{\mathbf{k}\uparrow} c^{\dagger}_{-\mathbf{k}\downarrow}) \, |0\rangle \, , \tag{1.1}$$

where $\mathbf{k}$ is the wave-vector of an electron and $c_{\mathbf{k}\sigma}$ is the annihilation operator for an electron with spin projection $\sigma = \uparrow, \downarrow$. The coefficients $v_{\mathbf{k}}$ and $u_{\mathbf{k}}$ are expansion coefficients and obey $|u_{\mathbf{k}}|^2 + |v_{\mathbf{k}}|^2 = 1$. Furthermore $|v_{\mathbf{k}}|^2$ gives the probability of a pair $(\mathbf{k}\uparrow, -\mathbf{k}\downarrow)$ being occupied while $|u_{\mathbf{k}}|^2 = 1 - |v_{\mathbf{k}}|^2$ is the probability for a state being unoccupied. To find the value of $v_{\mathbf{k}}$ and $u_{\mathbf{k}}$ there are different methods that can be used. The variational method was used when BCS first presented the BCS theory [9], however, in this case we will use a canonical transformation which is presented below.

A general Hamiltonian for an s-wave superconductor considered in the BCS theory is

$$H_{BCS} = \sum_{\mathbf{k}\sigma} \xi_{\mathbf{k}} c^{\dagger}_{\mathbf{k}\sigma} c_{\mathbf{k}\sigma} + \sum_{\mathbf{k}\mathbf{k}'} V_{\mathbf{k}\mathbf{k}'} c^{\dagger}_{\mathbf{k}\uparrow} c^{\dagger}_{-\mathbf{k}\downarrow} c_{-\mathbf{k}'\downarrow} c_{\mathbf{k}'\uparrow}, \tag{1.2}$$

where $\xi_{\mathbf{k}} = \epsilon_{\mathbf{k}} - \mu$ is the energy of a single electron measured from the chemical potential, μ, and $V_{\mathbf{k}\mathbf{k}'}$ is the coupling strength. The Hamiltonian describes the interaction between Cooper pairs and thus the ground state of the BCS Hamiltonian could be expected to be the BCS ground state, Eq. (1.1), since it is a superposition of states filled with an integer number of Cooper pairs [11]. A consequence of this is that the pair operators $c^{\dagger}_{\mathbf{k}\uparrow} c^{\dagger}_{-\mathbf{k}\downarrow}$ and $c_{\mathbf{k}\uparrow} c_{-\mathbf{k}\downarrow}$ has a finite ground state expectation value, thus $\langle c^{\dagger}_{\mathbf{k}\uparrow} c^{\dagger}_{-\mathbf{k}\downarrow} \rangle$ and $\langle c_{\mathbf{k}\uparrow} c_{-\mathbf{k}\downarrow} \rangle$ are non-zero and due to the large number of particles involved, fluctuations around these are small [9]. Because of this it is useful to make a mean-field approximation. This means that we can write the density operators as a sum of its expectation value and a term describing small fluctuations around it [11]

$$c_{-\mathbf{k}\downarrow} c_{\mathbf{k}\uparrow} = \langle c_{-\mathbf{k}\downarrow} c_{\mathbf{k}\uparrow} \rangle + \delta_{\mathbf{k}} \tag{1.3}$$

By re-writing the Hamiltonian in Eq. (1.2) with Eq. (1.3) and neglecting terms that are bilinear in $\delta_{\mathbf{k}}$ we obtain the mean-field BCS Hamiltonian

$$H^{MF}_{BCS} = \sum_{\mathbf{k}\sigma} \xi_{\mathbf{k}} c^{\dagger}_{\mathbf{k}\sigma} c_{\mathbf{k}\sigma} + \sum_{\mathbf{k}\mathbf{k}'} V_{\mathbf{k}\mathbf{k}'} \left[c^{\dagger}_{\mathbf{k}\uparrow} c^{\dagger}_{-\mathbf{k}\downarrow} \langle c_{-\mathbf{k}'\downarrow} c_{\mathbf{k}'\uparrow} \rangle + c_{-\mathbf{k}'\downarrow} c_{\mathbf{k}'\uparrow} \langle c^{\dagger}_{\mathbf{k}\uparrow} c^{\dagger}_{-\mathbf{k}\downarrow} \rangle - \langle c^{\dagger}_{\mathbf{k}\uparrow} c^{\dagger}_{-\mathbf{k}\downarrow} \rangle \langle c_{-\mathbf{k}'\downarrow} c_{\mathbf{k}'\uparrow} \rangle \right]. \tag{1.4}$$

The last term in the Hamiltonian is a constant and can be included in the chemical potential. We define the superconducting order parameter as

$$\Delta_{\mathbf{k}} = -\sum_{\mathbf{k}'} V_{\mathbf{k}\mathbf{k}'} b_{\mathbf{k}'} = -\sum_{\mathbf{k}'} V_{\mathbf{k}\mathbf{k}'} \langle c_{-\mathbf{k}'\downarrow} c_{\mathbf{k}'\uparrow} \rangle. \tag{1.5}$$

Based on this (and some relabelling of subscripts) the mean-field BCS Hamiltonian can be written as

$$H^{MF}_{BCS} = \sum_{\mathbf{k}\sigma} \xi_{\mathbf{k}} c^{\dagger}_{\mathbf{k}\sigma} c_{\mathbf{k}\sigma} - \sum_{\mathbf{k}} (\Delta_{\mathbf{k}} c^{\dagger}_{\mathbf{k}\uparrow} c^{\dagger}_{-\mathbf{k}\downarrow} + \Delta^{*}_{\mathbf{k}} c_{-\mathbf{k}\downarrow} c_{\mathbf{k}} \downarrow). \tag{1.6}$$

The Hamiltonian can be diagonalized by a linear Bogoliubov transform:

$$\begin{pmatrix} \gamma_{\mathbf{k}\uparrow} \\ \gamma^{\dagger}_{-\mathbf{k}\downarrow} \end{pmatrix} = \begin{pmatrix} u^{*}_{\mathbf{k}} & v_{\mathbf{k}} \\ -v^{*}_{\mathbf{k}} & u_{\mathbf{k}} \end{pmatrix} \begin{pmatrix} c_{\mathbf{k}\uparrow} \\ c^{\dagger}_{-\mathbf{k}\downarrow} \end{pmatrix} \tag{1.7}$$

and the inverse of this transform is given by

$$\begin{pmatrix} c_{\mathbf{k}\uparrow} \\ c^{\dagger}_{-\mathbf{k}\downarrow} \end{pmatrix} = \begin{pmatrix} u_{\mathbf{k}} & -v_{\mathbf{k}} \\ v^{*}_{\mathbf{k}} & u_{\mathbf{k}} \end{pmatrix} \begin{pmatrix} \gamma_{\mathbf{k}\uparrow} \\ \gamma^{\dagger}_{-\mathbf{k}\downarrow} \end{pmatrix}, \tag{1.8}$$

where the coefficients $u_{\mathbf{k}}$ and $v_{\mathbf{k}}$ are the same as those in the BCS ground state, Eq. (1.2), and satisfy $|u_{\mathbf{k}}|^2 + |v_{\mathbf{k}}|^2 = 1$. The operator, $\gamma_{\mathbf{k}\uparrow} = u^{*}_{\mathbf{k}} c_{\mathbf{k}\uparrow} + v_{\mathbf{k}} c^{\dagger}_{-\mathbf{k}\downarrow}$ creates a superposition of an electron with $\mathbf{k}\uparrow$ and an electron with $-\mathbf{k}\downarrow$. The net effect of the operator is to reduce the momentum by $\mathbf{k}$ and reduce the total spin by $\hbar/2$. By inserting these operators into Eq. (1.6) the Hamiltonian is found to be diagonal if [11]

$$|v_{\mathbf{k}}|^2 = 1 - |u_{\mathbf{k}}|^2 = \frac{1}{2}\left(1 - \frac{\xi_{\mathbf{k}}}{E_{\mathbf{k}}}\right), \tag{1.9}$$

where

$$E_{\mathbf{k}} \equiv \sqrt{\xi^2_{\mathbf{k}} + |\Delta_{\mathbf{k}}|^2}. \tag{1.10}$$

The diagonal Hamiltonian is

$$H^{MF}_{BCS} = \sum_{\mathbf{k}} E_{\mathbf{k}} (\gamma^{\dagger}_{\mathbf{k}\uparrow}\gamma_{\mathbf{k}\uparrow} + \gamma^{\dagger}_{\mathbf{k}\downarrow}\gamma_{\mathbf{k}\downarrow}) + \text{constant terms}. \tag{1.11}$$

The dispersion relation, given in Eq. (1.10) is shown in Fig. 1.1. As seen there is a gap with the size of $2|\Delta_{\mathbf{k}}|$ opened up in the excitation spectrum and thus there is a smallest required energy of $2|\Delta_{\mathbf{k}}|$ for fermionic excitations. It will later be seen that MBSs will emerge in the middle of the superconducting gap.

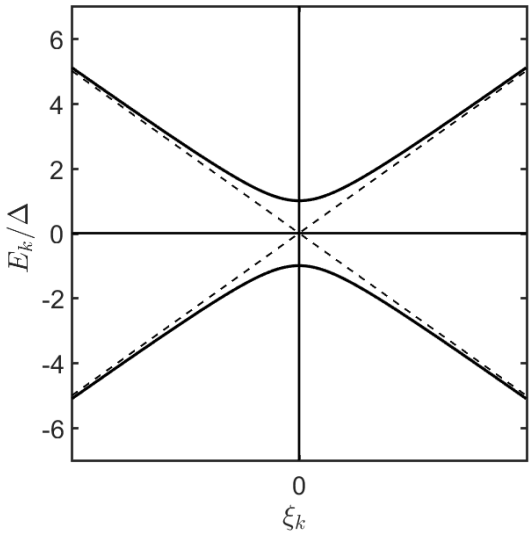

FIG. 1.1. (Solid line) The excitation spectrum, Eq. (1.10) of a superconductor compared to the spectrum of a normal metal (dashed line). As seen, a gap is opened up in the excitation spectrum of the superconductor.

1.4 Spin-orbit coupling

A key ingredient for realizing MBS in a nanowire is the spin-orbit (SO) coupling. The SO coupling is needed to realize so called topological superconductivity in the nanowire [12]. The SO coupling is a relativistic effect that leads to for example a spin splitting of the energy bands in a semiconductor. If we consider an electron moving with a momentum, $\mathbf{p}$, we can make a Lorentz transformation to the reference frame of the electron. The Lorentz transform of the electric and magnetic field is given by [13]

$$\mathbf{E} \rightarrow \mathbf{E}' = \mathbf{E} + \mathbf{v} \times \mathbf{B} \tag{1.12a}$$

$$\mathbf{B} \rightarrow \mathbf{B}' = \mathbf{B} - \frac{1}{c^2}\mathbf{v} \times \mathbf{E}, \tag{1.12b}$$

where $\mathbf{E}$ is the electric field, $\mathbf{B}$ is the magnetic field, $\mathbf{v}$ is the velocity of the electron and c is the speed of light. The primes denote the reference frame of the electron. Due to this, a particle moving in an electric field will experience a magnetic field, $\mathbf{B}' = -\frac{1}{c^2}\mathbf{v} \times \mathbf{E}$. This magnetic field will interact with the magnetic moment of the electron and the energy due to this interaction can be included in the Hamiltonian by adding the term

$$\hat{H}_{SO} = -\boldsymbol{\mu} \cdot \mathbf{B}' = \frac{g\mu_B}{c^2}(\mathbf{v} \times \mathbf{E}) \cdot \mathbf{S}. \tag{1.13}$$

where $\mathbf{S}$ is the spin operator, μ_B is the Bohr magneton and g is the Landé g-factor. This can be re-written by using $\mathbf{p} = m\mathbf{v}$ and $\mathbf{S} = \frac{\hbar}{2}\sigma$ for two-component spin systems where σ is a vector containing the Pauli matrices. Substituting this into Eq. (1.13), using that $\mu_B = \frac{e}{2m}$ and changing order of the cross product we obtain

$$\hat{H}_{SO} = \frac{g\mu_B\hbar}{2mc^2}\boldsymbol{\sigma} \cdot (\mathbf{p} \times \mathbf{E}). \tag{1.14}$$

From this equation we see that the energy splitting given by the spin-orbit interaction is proportional to both the momentum of the particles as well as the electric field. Due to the small pre-factors this effect is going to be very small if not the momentum or the electric field is very large. If we consider a metal where $v_F \approx 10^6\,\mathrm{m/s}$ [10] and assume an electric field of $10^6\,\mathrm{V/m}$, which is of the order as for which air break down, this results in an energy of approximately $10^{-10}\,\mathrm{eV}$. This shows that huge electric fields is needed to produce a very small energy splitting.

Now we consider the case of SO coupling in semiconductors. In general the electric field is given by $\mathbf{E} = -\nabla V$ [13] where V is the crystal potential. This gives a SO field

$$\mathbf{w}(\mathbf{p}) = \frac{g\mu_B}{2mc^2}(\nabla V \times \mathbf{p}). \tag{1.15}$$

It is known from [14] that SO coupling is invariant under time reversal symmetry. Thus we consider what happens when time-reversing $\mathbf{p}$ and $\boldsymbol{\sigma}$. The momentum operator changes sign under time reversal, $\mathbf{p} \to -\mathbf{p}$ [14]. To find the time-reversal of the spin angular momentum we define the time-reversal operator, T, as [15]

$$T = \sigma_y K \tag{1.16}$$

where K is the complex conjugation operator and σ_y the Pauli matrix in the y direction. The time-reversal of the spin angular momentum is then found to be $T^\dagger \boldsymbol{\sigma} T = -\boldsymbol{\sigma}$. From this it then follows that

$$\mathbf{w}(p) \cdot \boldsymbol{\sigma} = -\mathbf{w}(-p) \cdot \boldsymbol{\sigma}. \tag{1.17}$$

This implies that $-\mathbf{w}(\mathbf{p}) = \mathbf{w}(-\mathbf{p})$ which is odd in momentum. This can only happen for semiconductors that are asymmetric under space inversion [16]. There are two main effects causing the space inversion asymmetry. The bulk inversion asymmetry (BIA) was pointed out by Dresselhaus after noticing that zinc-blende structures lacked a centre of inversion [17]. Close to the Γ point the SO coupling takes the form [16]

$$\hat{H}_{D_3} = \frac{\gamma}{\hbar}((p_y^2 - p_z^2)p_x\sigma_x + c.p.), \tag{1.18}$$

where γ is a material dependent parameter and $c.p.$ denotes circular permutation of indices. For semiconductor quantum structures the inversion symmetry can also be lifted, additionally to the BIA, by structure inversion asymmetry (SIA). The SIA is due to the asymmetry of the confining potential $V(\mathbf{r})$. This was taken into account by Bychakov and Rashba who then proposed the following Hamiltonian for SO coupling [16]

$$\hat{H}_R = \frac{\alpha_R}{\hbar}(\mathbf{r} \times \mathbf{p}) \cdot \boldsymbol{\sigma}, \tag{1.19}$$

where α_R is the Rashba parameter and is material dependent. The Rashba parameter replaces the pre-factor in Eq. (1.14) and typically $\alpha_R/\hbar >> \mu_B E_z/mc$ where E_z is the electric field in the z-direction, which is in this case the direction of the asymmetry. This relation then states that the SO coupling is much stronger in a semiconductor than it is for a free electron and compared to the previous calculated energy splitting, the Rashba spin-orbit coupling gives an

energy splitting around 0.1 meV [18], which is 10^6 times larger than that of an free electron.

For a one-dimensional electron gas (1DEG) directed along the x-axis with an electric field pointing in along the z-axis this reduces to $\hat{H}_R = \alpha_R k_x \sigma_y$. The total Hamiltonian for a 1DEG then reads

$$\hat{H}_{1DEG} = \epsilon_k + \alpha_R k_x \sigma_y. \tag{1.20}$$

where $\epsilon_k = \frac{k_x^2}{2m}$. This Hamiltonian is easily diagonalized resulting in

$$E_k = \epsilon_k \pm \alpha_R k_x. \tag{1.21}$$

The dispersion relation is shown in Fig. 1.2. The free electron parabola is split into two shifted parabolas representing the spin splitting between $k_{x\uparrow}$ and $k_{x\downarrow}$. It should be noted that due to the Hamiltonian, Eq. (1.20), spin up and spin down refers to spin up and spin down in the y-direction.

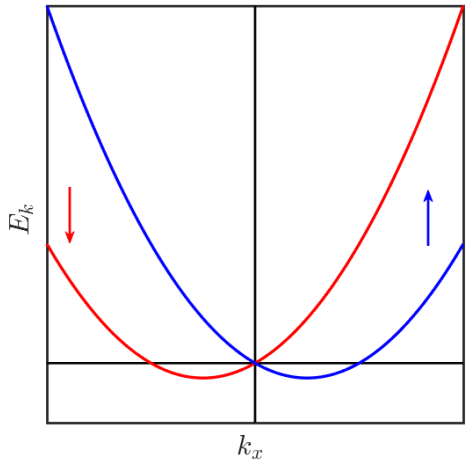

FIG. 1.2. The dispersion relation, Eq. (1.21) for a 1DEG with Rashba spin-orbit coupling. The arrows represent the spin carried by the two different bands. In this case spin up and spin down represent spin up and spin down in the y-direction.

1.5 Majorana Bound States

The criteria for a state to be considered a MBS is that the operator creating a MBS is equal to the operator annihilating the MBS. Thus

$$\gamma = \gamma^\dagger, \tag{1.22}$$

where γ ($\gamma^\dagger$) is the annihilation (creation) operator of a MBS. A consequence of this is that the MBS will then be a state that is its 'own hole'. For an excitation involving electrons and holes states to be its own anti-state it is required that the excitation is an equal superposition of electron and hole states. An operator that creates a state which is a superposition with an equal part of electrons and holes and that also fulfills Eq. (1.22) is

$$\gamma = c + c^\dagger, \tag{1.23}$$

where c ($c^\dagger$) is a fermion annihilation (creation) operator. From the structure of this operator it is clear that we should look for excitations in superconductors. This can be realized by the fact that the wavefunctions of Bogliubov quasiparticles have an electron and a hole part [9]. If we for a moment drop the spin indices then, in terms of creation and annihilation operators, the Bogoliubov quasiparticle is written as

$$\gamma = uc^\dagger + vc, \tag{1.24}$$

where the prefactors u and v are given by the energy of the Bogoliubov quasiparticle excitation. Excitations happening far above the superconducting gap can be well approximated to behave like an electron and thus $|u| \approx 1$ and $|v| \approx 0$. Similar for excitations happening in the Fermi sea far below the superconducting gap, these can be well approximated with a hole and $|u| \approx 0$ and $|v| \approx 1$. The amplitude of the creation and annihilation operator in Eq. (1.23) is equal and therefore if Eq. (1.24) shall describe a MBS we require that $u = v$. If we consider the energy dependence of u and v we could expect that $u = v$ should be in between excitations looking just like an electron and excitations looking just like a hole. This means that excitations with $u = v$ is in the mid-gap, which corresponds to $E = \mu$ in a superconducting system. Now, in the standard theory Bogoliubon quasiparticles are given by (Eq. (1.7))

$$\gamma = uc^\dagger_\uparrow + vc_\downarrow. \tag{1.25}$$

The spin indices makes this operator different from Eq. (1.24) and since the direction of the spin indices is different the requirement for being a Majorana operator, $\gamma = \gamma^\dagger$, cannot be fulfilled. Due to this we cannot have MBS in superconducting systems of s-wave type.

If we instead consider pairing between spinless fermions this is no longer a problem. There is an immediate consequence of this assumption. In the standard BCS theory the wave functions of the Cooper pair must be antisymmetric due to the Pauli principle. The condition of having an antisymmetric wave function is fulfilled by the electrons being in an antisymmetric spin-singlet configuration in an s-wave superconductor. However, for a spinless superconductor the orbital wave function must be antisymmetric. Due to this the we cannot have an s-wave superconductor since it has a symmetric orbital wave function. The simplest option is a superconductor with p-wave pairing (pairing of electrons with same spin), which is antisymmetric in the orbital wave function. As a conclusion from the above given arguments, MBSs are mid-gap excitations in p-wave superconducting systems.

In this section a short introduction to what a MBS is and where it can be found has been given. In the next sections a toy model of where MBSs occur as well as a model that can be realized in reality will be presented.

1.6 Kitaev chain

A realistic model for MBSs is presented in the next section, however, here we present a simple model to realize MBSs. This is the Kitaev model or the Kitaev chain. The Kitaev chain is a

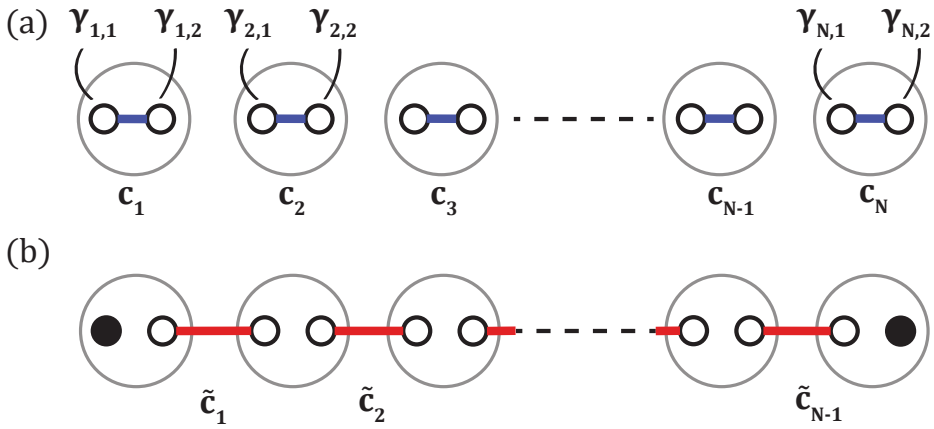

FIG. 1.3. The Kitaev model for two special cases. (a) Case 1, The Majorana operators on same sites, c_i is paired together and... (b) Case 2, Majorana operators on adjacent sites pair and form $\tilde{c}_i$. The Majorana operators the ends of the chain (filled black circles) are left out and can form a highly non-local state that requires zero energy to be occupied, a so called Majorana zero mode.

one dimensional model of a "quantum wire" consisting of N sites [19]. The model assumes that only one spin direction is present. The requirement of superconductivity is taken into account by an induced p-wave superconductivity. The Hamiltonian for the Kitaev chain consisting of N sites reads

$$H = \sum_i \left(-t(c_i^\dagger c_{i+1} + c_{i+1}^\dagger c_i) - \mu(c_i^\dagger c_i - \frac{1}{2}) + \Delta c_i c_{i+1} + \Delta^* c_{i+1}^\dagger c_i^\dagger \right), \tag{1.26}$$

where t is the hopping amplitude, μ the chemical potential and Δ is the induced superconducting gap. The Majorana operators are then defined as

$$\gamma_{i,1} = c_i^\dagger + c_i, \quad \gamma_{i,2} = i(c_i^\dagger - c_i), \tag{1.27}$$

where $i = 1, 2, ..., N$. These operators are Majorana operators since they satisfy Eq. (1.22). The fermionic creation and annihilation operators are, in terms of Majorana operators written as

$$c_i = \frac{1}{2}(\gamma_{i,1} + i\gamma_{i,2}), \quad c_i^\dagger = \frac{1}{2}(\gamma_{i,1} - i\gamma_{i,2}). \tag{1.28}$$

These operators say that mathematically we can split a fermionic state into two MBSs. The Hamiltonian in Eq. (1.26) can be re-written in terms of Majorana operators using Eq. (1.28). This gives

$$H = \frac{i}{2} \sum_i \left(-\mu\gamma_{i,1}\gamma_{i,2} + (t + |\Delta|)\gamma_{i,2}\gamma_{i+1,1} + (-t + |\Delta|)\gamma_{i,1}\gamma_{i+1,2} \right). \tag{1.29}$$

Due to the structure of the Hamiltonian there are two special cases to consider, *Case 1*, when $|\Delta| = t = 0$ and $\mu < 0$ and *Case 2*, when $|\Delta| = t > 0$ and $\mu = 0$.

Case 1 This case is trivial and leads to

$$H = -\mu \sum_i (c_i^\dagger c_i - \frac{1}{2}) = -\frac{i\mu}{2} \sum_i \gamma_{i,1}\gamma_{i,2}. \tag{1.30}$$

The Hamiltonian consists of paired Majorana operators that lives on the same site, i, and form a ground state with occupation number zero. This is presented graphically in Fig. 1.3a.

Case 2 Given $|\Delta| = t > 0$ and $\mu = 0$ the Hamiltonian, Eq. (1.29) becomes

$$H = it \sum_i \gamma_{i,2}\gamma_{i+1,1}. \tag{1.31}$$

Now Majorana opearators from two adjacent sites couple (presented graphically in Fig. 1.3.b). One can define a new fermion operator consisting of Majorana operators from adjacent sites

$$\tilde{c_i} = \frac{1}{2}(\gamma_{i+1,1} + i\gamma_{i,2}). \tag{1.32}$$

In terms of Majorana operators these can be expressed as

$$\gamma_{i,2} = \tilde{c_i}^\dagger + \tilde{c_i}, \quad \gamma_{i+1,1} = i(c_i^\dagger - c_i). \tag{1.33}$$

Taking these operators and inserting them in Eq. (1.31) leads to

$$H = 2 \sum_i^{N-1} (\tilde{c}_i^\dagger \tilde{c}_i - \frac{1}{2}). \tag{1.34}$$

One can notice the absence of the operators $\gamma_{1,1}$ and $\gamma_{N,2}$ in the Hamiltonian and thus they remain unpaired. These two operators can be combined to form a new fermionic operator

$$\tilde{c_N} = \frac{1}{2}(\gamma_{1,1} + \gamma_{N,2}). \tag{1.35}$$

Since the operators $\gamma_{1,1}$ and $\gamma_{N,2}$ live on the opposite ends of the chain, Eq. (1.35) forms a state that is far from local. Since neither $\gamma_{1,1}$ nor $\gamma_{N,2}$ is included in the Hamiltonian it follows that $[\gamma_{1,1}, H] = [\gamma_{N,2}, H] = 0$. Due to this there exist one fermionic state at zero energy, which can be either empty or occupied. Due to this the the ground state of the Kitaev model is two-fold degenerate.

In this section we have considered two special cases of the Kitaev chain where one of the cases illustrates the formation of non-local states at the end of the chain. There are other settings of the parameters also resulting in end states but this will not be shown here (this can e.g be found in [19]), instead an argument for that they exist will be given. Given these parameters the system is said to be in the topologically non-trivial phase. A system in the topologically non-trivial phase has states at zero energy, separated from the rest by an energy gap. We consider

$$H_{tot} = H_K + \lambda H_1, \tag{1.36}$$

where H_K is the Hamiltonian of the Kitaev chain with $t = \Delta$ and $\mu = 0$, and H_1 is an arbitrary

Hamiltonian with the same symmetries as the Kitaev chain [19]. If $\lambda = 0$ then $H_{tot} = H_K$ and of course host MBSs. Now, by increasing λ the energy gap may either remain open or close. As long as the gap stays open, while continously changing λ, the topology is preserved and the system will host MBSs. This means that if we can make a continous transformation between two systems without closing the gap the topology is preserved and if one of the systems host MBSs then so will the other [2].

Chapter 2

Model

2.1 Nanowire with spin-orbit coupling and proximity induced superconductivity

In this section we consider a system that resembles the Kitaev chain but which can be realized in experimental setups. The system is a nanowire with SO coupling, proximity induced superconductivity and subjected to a magnetic field. The experimental setup is presented in Fig. 2.1. The nanowire is directed along the x-axis. The applied magnetic field, B is directed along the z-axis. A set of gate potentials is applied beneath the wire and controls the chemical potential in the wire.

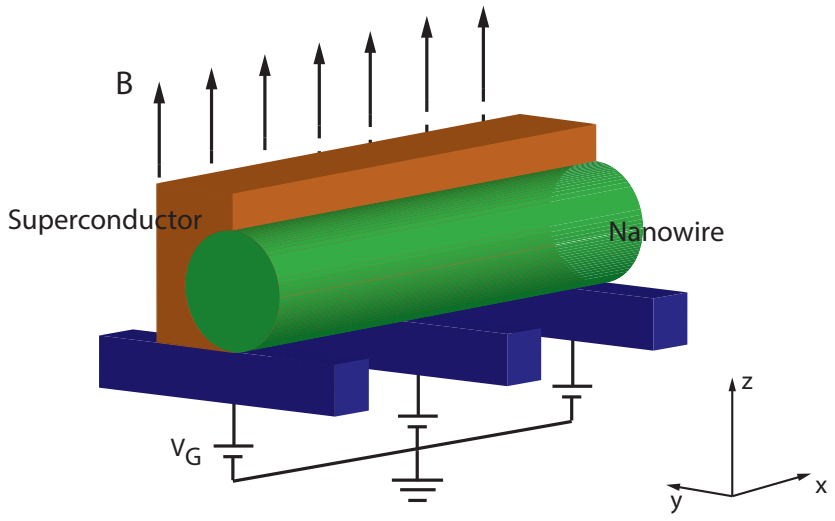

FIG. 2.1. Nanowire with SO coupling in proximity with superconductor. The wire is directed along the x-direction. The superconductor induces superconductivity in the nanowire via tunnelling of Cooper-pairs from the superconductor into the nanowire. The applied magnetic field is B and is in the z-direction. The system is connected to a set of gate electrodes, which controls the chemical potential in the nanowire.

The Hamiltonian describing the low energy physics of a strictly one-dimensional semiconductor nanowire with SO coupling and induced superconductivity is [20, 3]

$$H = \int \Psi^\dagger(x)\mathcal{H}\Psi(x)dx, \tag{2.1}$$

where $\mathcal{H}$ is usually denoted the Bogoliubov-de Gennes (BdG) Hamiltonian. Since we are considering a system with superconductivity it is convenient to include both electrons and holes. This is taken care of by working with the so-called Nambu spinors

$$\Psi = (\psi_\uparrow, \psi_\downarrow, \psi_\downarrow^\dagger, -\psi_\uparrow^\dagger)^T. \tag{2.2}$$

Here $\psi_{\uparrow,(\downarrow)}(x)$ ($\psi^\dagger_{\uparrow,(\downarrow)}(x)$) annihilates (creates) electrons with given spin projection at position x. Since matrices acting on Nambu spinors must be 4×4 matrices we introduce Pauli matrices, τ_i, acting in particle-hole space. The Pauli matrices acting in particle-hole space have the same form as the Pauli matrices acting in spin space, σ_i. The 4×4 matrices acting on spin and particle-hole space are given by the tensor product, $\tau_i \otimes \sigma_i$ (suppressed to $\tau_i\sigma_i$). The BdG Hamiltonian is then given by

$$\mathcal{H} = \left[\frac{p^2}{2m} - \mu(x)\right]\tau_z + \alpha p \sigma_x \tau_z + V_Z \sigma_z + \Delta(x)\tau_x, \tag{2.3}$$

where p is the momentum operator and μ is the chemical potential. The second term in the Hamiltonian describes the SO coupling of the nanowire and α is the Rashba SO coupling constant. The third term describes the Zeeman energy, V_Z, due to the applied magnetic field. $V_Z = \frac{1}{2} g \mu_B B$ where B is the strength of the applied magnetic field. The induced superconductivity in the wire is described by the fourth term where $\Delta(x) = \Delta$ is the proximity induced superconducting gap. It should be noted that terms including only σ_i and τ_i should be understood as $\sigma_i\tau_1$ and $\sigma_1\tau_i$ where σ_1 and τ_1 are the identity matrix in spin and particle-hole space respectively. Furthermore, since we have introduced particle-hole space we have doubled the number of solutions. Since the number of independent solutions cannot be changed there must be a symmetry between the original states and the ones we get from doubling the number of states. The symmetry is the particle-hole symmetry. This means that for every energy state, E_i, there exist a state E_j such that $E_j = -E_i$ [2]. Diagonalization of the BdG Hamiltonian gives

$$E_\pm^2 = (\frac{p^2}{2m} - \mu)^2 + V_Z^2 + \Delta^2 + (\alpha p)^2 \pm 2\sqrt{V_Z^2\Delta^2 + V_Z^2(\frac{p^2}{2m} - \mu) + (\alpha p)^2(\frac{p^2}{2m} - \mu)^2}. \tag{2.4}$$

The excitation spectrum is plotted for various values of the parameters V_Z, Δ and μ in Fig. 2.2. The spectrum is as expected not gapped when $\Delta = 0$ (Fig. 2.2a). The Zeeman term can, however, open a gap at $p = 0$ but there still exist other momenta for which the gap is closed (Fig. 2.2b). By letting $\Delta \neq 0$ the spectrum becomes fully gapped as shown in Fig. 2.2c. For $p = 0$ the energy of the lower branch of the excitation spectrum is given by

$$E_0 = E(p = 0) = \sqrt{V_Z^2 + \Delta^2 + \mu^2 - 2\sqrt{V_Z^2\Delta^2 + V_Z^2\mu^2}} = |V_Z - \sqrt{\Delta^2 + \mu^2}|. \tag{2.5}$$

For the case when $V_Z < \sqrt{\Delta^2 + \mu^2}$ the gap is dominated by the pairing term, Figs. 2.2a to 2.2c and 2.2f. When $V_Z = \sqrt{\Delta^2 + \mu^2}$, E_0 vanish and a phase transition occurs, which can be seen in Figs. 2.2d and 2.2e. In the region, $V_Z > \sqrt{\Delta^2 + \mu^2}$ the excitation spectrum is dominated by the magnetic field and the system is in the topologically non-trivial phase and thus it can support MBSs. The argument for the existence of the topologically non-trivial phase in nanowires with SO coupling and induced superconductivity is given in the next section.

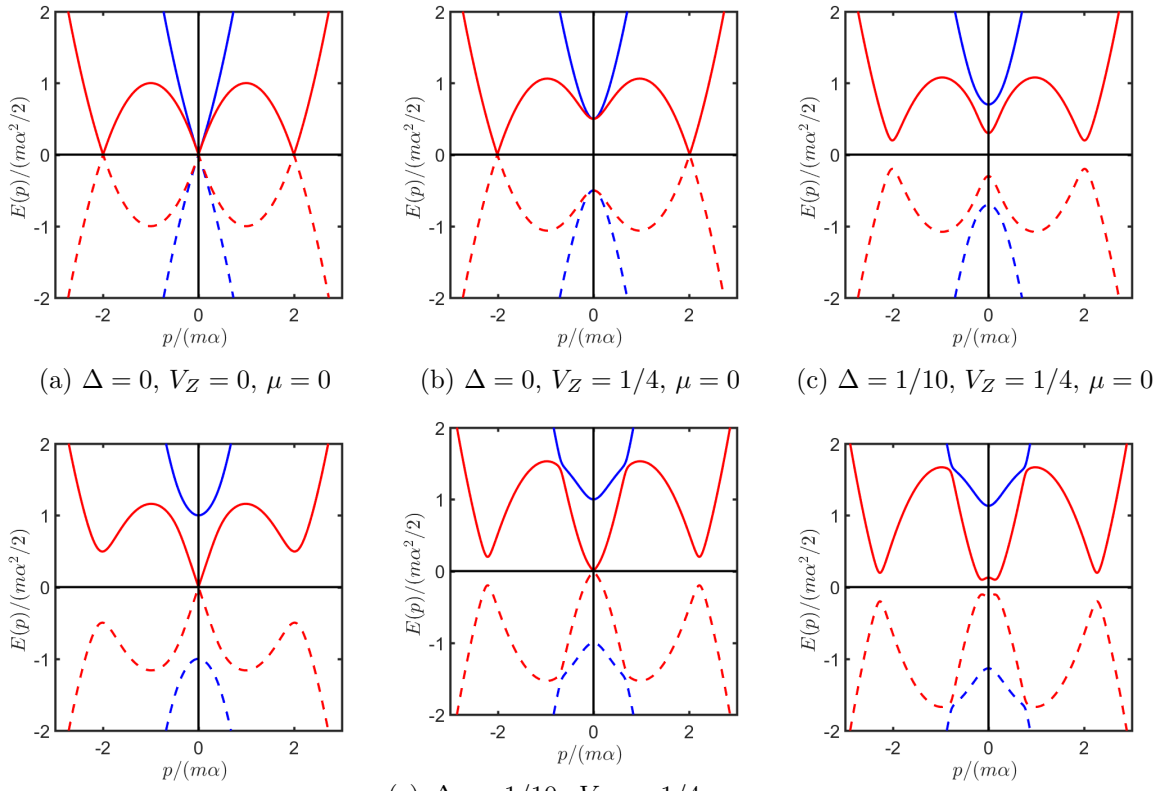

(a) $\Delta = 0$, $V_Z = 0$, $\mu = 0$ (b) $\Delta = 0$, $V_Z = 1/4$, $\mu = 0$ (c) $\Delta = 1/10$, $V_Z = 1/4$, $\mu = 0$

(d) $\Delta = 1/4$, $V_Z = 1/4$, $\mu = 0$ (e) $\Delta = 1/10$, $V_Z = 1/4$, $\mu = \sqrt{21}/20$ (f) $\Delta = 1/10$, $V_Z = 1/4$, $\mu = 0.3$

FIG. 2.2. The plots show the excitation spectrum, Eq. (2.5), for various values of the parameters V_Z, Δ and μ. The red line shows the lower branch of the spectrum while the blue shows the upper branch. The solid (dashed) lines are the electron (hole) states (a) $\Delta = 0$, $B = 0$, $\mu = 0$. (b) $\Delta = 0$, $V_Z = 1/4$, $\mu = 0$. (c) $\Delta = 1/10$, $V_Z = 1/4$, $\mu = 0$. (d) $\Delta = 1/4$, $V_Z = 1/4$, $\mu = 0$. (e) $\Delta = 1/10$, $V_Z = 1/4$, $\mu = \sqrt{21}/20$. (f) $\Delta = 1/10$, $V_Z = 1/4$, $\mu = 0.3$.

2.1.1 Majorana bound states in nanowire with spin-orbit coupling and proximity induced superconductivity

In this section it is proved that in certain limits the nanowire with SO coupling reduces to the one dimensional Kitaev model. The continous model of the Kitaev chain, Eq. (1.26) is given by [15]

$$H_{p-wave} = \int dx \left\{ \psi^\dagger(x) \left(\frac{p^2}{2m} + \mu \right) \psi(x) + \Delta^* [\psi^\dagger(x) \partial_x \psi^\dagger(x) + h.c] \right\}. \tag{2.6}$$

The BdG Hamiltonian associated with this Hamiltonian is [15]

$$\mathcal{H} = \left(\frac{p^2}{2m} - \mu \right) \tau_z + \Delta' p \tau_x, \tag{2.7}$$

and the spectrum of this Hamiltonian is given by

$$E_k = \pm \left[\left(\frac{\hbar^2 k^2}{2m} - \mu \right)^2 + \Delta'^2 k^2 \right]. \tag{2.8}$$

Everywhere, except for the case when $\mu = 0$ and $k = 0$, the spectrum is gapped. Since this is just a continuous version of the Kitaev model there exist solutions that are MBSs. Now to show that the nanowire with SO coupling also host MBSs we want to map the Hamiltonian, Eq. (2.3), onto Eq. (2.7). We consider the case for a strong Zeeman field and a chemical potential far below the spin-down parabola. In this case one can derive an effective low-energy Hamiltonian by projecting out the high-energy states belonging to the spin-down parabola. If we neglect the SO coupling and define zero energy at the bottom of the band this results in that the magnetic field produces a shift in the chemical potential and we can write

$$H = \left(\frac{p^2}{2m} - (V_Z + \mu)\right)\tau_z + \Delta\tau_x \to \left(\frac{p^2}{2m} - \mu\right)\tau_z + \Delta\tau_x. \tag{2.9}$$

In the absence of spin-orbit interaction the low-energy subspace is spanned by the spin-up electron and the spin-up hole

$$|e\uparrow\rangle = [1,0,0,0]^T \quad |h\uparrow\rangle = [0,0,0,1]^T. \tag{2.10}$$

From this it follows that $\langle e\uparrow|\Delta\tau_x|e\uparrow\rangle = \langle e\uparrow|\Delta\tau_x|h\uparrow\rangle = \langle h\uparrow|\Delta\tau_x|e\uparrow\rangle = \langle h\uparrow|\Delta\tau_x|h\uparrow\rangle = 0$. This means that we cannot have proximity induced superconductivity with spin-singlet Cooper pairs in a system that is perfectly spin-polarized. Now we include the SO coupling. This is done by using first-order perturbation theory which is valid since $V_Z > \alpha p$ around the points where the energy gap open and close. This modifies the low-energy spinors such that

$$|e\uparrow\rangle = [1,-\alpha p/2B,0,0]^T \quad |h\uparrow\rangle = [0,0,-\alpha p/2B,1]^T. \tag{2.11}$$

By repeating the calculations for the matrix elements of the pairing terms we obtain

$$\langle e\uparrow|\Delta\tau_x|h\uparrow\rangle = \langle h\uparrow|\Delta\tau_x|e\uparrow\rangle = -\frac{\alpha p}{B}\Delta, \tag{2.12a}$$

$$\langle e\uparrow|\Delta\tau_x|e\uparrow\rangle = \langle h\uparrow|\Delta\tau_x|h\uparrow\rangle = 0. \tag{2.12b}$$

Due to the low-energy projection the Hamiltonian becomes

$$H \simeq \left(\frac{p^2}{2m} - \mu\right)\tau_z - \frac{\alpha p}{B}\Delta\tau_x. \tag{2.13}$$

By comparing this Hamiltonian with the Hamiltonian given for the continuous model of the p-wave superconductor, Eq. (2.7) we see that if we chose $\Delta' = \frac{\alpha\Delta}{B}$ the projected low-energy Hamiltonian of the nanowire with SO coupling maps onto the Hamiltonian of the continuous p-wave superconductor. Since the p-wave superconductor hosts MBS so will also the nanowire with SO coupling. Furthermore, as explained in Section 1.6 the system will host MBSs for all parameter values that can be reached when making a continuous transformation between these without ever closing the gap.

2.2 Numerical model

When making the nanowire finite, $\mathbf{k}$ is no longer a good quantum number and the continuous Hamiltonian can no longer be diagonalized. To account for this we use a tight-binding model. The tight-binding Hamiltonian corresponding to Eq. (2.1) is given by [3]

$$H_{tot} = H_0 + H_{SOI} + H_Z + H_V + H_{SC}, \tag{2.14}$$

where H_0 describes the kinetic energy part of the nanowire, H_{SOI} the spin-orbit interaction in the nanowire, H_Z is the Hamiltonian for the applied magnetic field, H_V describes disorder in the nanowire and added gate potentials and H_{SC} is the Hamiltonian for the induced superconductivity in the nanonwire. The above described terms for a one-dimensional tight binding model with a lattice constant a are given by

$$H_0 = -t \sum_{i,\sigma} c^\dagger_{i+1,\sigma} c_{i,\sigma} + \mu \sum_{i,\sigma} c^\dagger_{i,\sigma} c_{i,\sigma}. \tag{2.15}$$

Here, i labels the lattice sites, μ is the chemical potential, $t_0 = \frac{\hbar^2}{2m^* a^2}$ is the effective hopping parameter and m^* is the effective mass. The Hamiltonian for the Rashba SO coupling is

$$H_{SOI} = \frac{i\alpha}{2} \sum_i \left[\bar{c}^\dagger_{i+1} \sigma_y \bar{c}_i + h.c. \right], \tag{2.16}$$

where $h.c.$ denotes Hermitian conjugate, $\bar{c}_i = (c_{i\uparrow}, c_{i\downarrow})^T$, α is the Rashba spin orbit coupling strength and $\alpha = \frac{\alpha_R}{a}$ where α_R is the Rashba parameter. The Hamiltonian describing the effect of the applied magnetic field in the nanowire is given by

$$H_Z = V_Z \sum_i \bar{c}^\dagger_i \boldsymbol{\sigma} \bar{c}_i, \tag{2.17}$$

where $\boldsymbol{\sigma}$ is a vector of Pauli matrices in the direction of the magnetic field, i.e. if the magnetic field is in the z-direction $\boldsymbol{\sigma} = (0, 0, \sigma_z)$. $V_Z = \frac{1}{2} g \mu_B B$ where B is the applied magnetic-field strength. Disorder, applied gate potentials or other effects causing a potential change in the wire is described by

$$H_V = \sum_i V_i c^\dagger_{i\sigma} c_{i\sigma}, \tag{2.18}$$

where V_i is the added potential change at site i. The proximity induced superconductivity is described by

$$H_{SC} = \Delta \sum_i (c^\dagger_{i\uparrow} c^\dagger_{i\downarrow} + c_{i\uparrow} c_{i\downarrow}), \tag{2.19}$$

where Δ is the proximity induced superconducting gap. The Nambu spinors in the tight-binding model are given by $\Psi_i = (c_{i\uparrow}, c_{i\downarrow}, c^\dagger_{i\downarrow}, -c^\dagger_{i\uparrow})^T$.

The matrix representation of a one-dimensional chain of a nanowire in the x-direction consisting on N lattice sites and with a magnetic field in the z-direction is a $N \times N$ block matrix where every block is a 4×4 matrix. The block matrix will only have elements on the diagonal and the

super-diagonal due to nearest neighbour hopping. The diagonal elements of the block matrix are written

$$H_{ii} = \begin{bmatrix} -\mu + V_Z + V_i & 0 & \Delta & 0 \\ 0 & -\mu - V_Z + V_i & 0 & \Delta \\ \Delta & 0 & \mu + V_Z - V_i & 0 \\ 0 & \Delta & 0 & \mu - V_Z - V_i \end{bmatrix}. \tag{2.20}$$

The Hamiltonian is Hermitian $H_{i,i+1} = H^{\dagger}_{i+1,i}$ and the matrices on the super-diagonal are given by

$$H_{i,i+1} = \begin{bmatrix} -t & \alpha/2 & 0 & 0 \\ -\alpha/2 & -t & 0 & 0 \\ 0 & 0 & t & -\alpha/2 \\ 0 & 0 & \alpha/2 & t \end{bmatrix}. \tag{2.21}$$

The spectrum is obtained by numerically diagonalising the matrix representation of the Hamiltonian. The number of lattice sites, n, that is used is determined by the length of the wire and the lattice constant, a. This is given by $n = \frac{L}{a} + 1$. The lattice parameter also controls the convergence. By making a smaller the convergence towards the exact energies can be increased. Since the matrix is a $4N \times 4N$ matrix there will be $4N$ eigenvalues corresponding to the allowed energy levels of the system. Due to the particle-hole symmetry it is convenient to label the energy levels between $-2N + 1$ and $2N$ and the two energy levels in the middle can thus be denoted E_0 and E_1. We denote the corresponding eigenvectors ψ_0 and ψ_1 and the MBSs that forms on the ends of an infinite wire $\mathbf{\Psi}_A$ and $\mathbf{\Psi}_B$. These states are given as $\mathbf{\Psi} = (u_\uparrow, u_\downarrow, v_\downarrow, -v_\uparrow)$ in spin and particle hole space. Here u and v are the amplitude of the electrons and the holes respectively. It can then be shown that a MBSs has $u_\uparrow = v^*_\downarrow$ and $u_\downarrow = v^*_\uparrow$ [21]. This is however not true when the system is made finite. The reason is that in a finite system the MBSs, as mentioned, starts to overlap, which means that the numerical solutions that we find from diagonalizing the tight-binding Hamiltonian will be a superposition of $\mathbf{\Psi}_A$ and $\mathbf{\Psi}_B$ with a finite energy [22]. This means that we can write

$$\psi_0 = \frac{1}{\sqrt{2}}(\mathbf{\Psi_A} + i\mathbf{\Psi_B}) \quad \psi_1 = \frac{1}{\sqrt{2}}(\mathbf{\Psi_A} - i\mathbf{\Psi_B}). \tag{2.22}$$

From this it then follows that the MBSs are generated by

$$\mathbf{\Psi}_A = \frac{1}{\sqrt{2}}(\psi_1 + \psi_0), \quad \mathbf{\Psi}_B = \frac{i}{\sqrt{2}}(\psi_1 - \psi_0). \tag{2.23}$$

Chapter 3

Results

Throughout this work, if otherwise not stated we investigate an indium arsenide (InAs) nanowire proximity-coupled to an aluminium (Al) superconductor. The induced superconducting gap in the wire is $\Delta = 0.25\,\text{meV}$. The Rashba parameter for InAs is $\alpha_R = 8 \cdot 10^{-12}\,\text{eVm}$ [23]. The energy dispersion relation of the tight-binding model is given by $E = \epsilon - 2t\cos(ka)$, which gives an energy band between $E = \epsilon - 2t$ and $E = \epsilon + 2t$ [24]. However, in Eq. (2.3) we have $\frac{p^2}{2m} - \mu$ with the bottom of the band energy band at $E = 0$. To ensure that the chemical potential is close to the bottom of the band in the tight binding model we choose $\mu = -2t$.

As will be seen, the main investigations made are how the energy eigenstates of the system vary as a function of Zeeman field, V_Z. For all cases V_Z is chosen to vary between 0 and 3Δ throughout the work. This corresponds to a magnetic field of 3.24 T given that $g \approx 8$ in InAs [18]. This is of special importance to know when designing the geometry of the superconductor since the superconducting state can be destroyed by a to strong magnetic field.

3.1 Homogeneous Nanowire

To understand what happens when a nanowire is made finite we start with investigating a homogeneous nanowire. Fig. 3.1a shows the twenty lowest energy states of the spectrum as a function of the Zeeman energy, V_Z, with the states in the middle of the spectrum marked in red. The length of the nanowire is $7\,\mu$m and can be considered long compared to those used in experiments [23]. When $V_Z = 0$ we have a fully gapped system with discrete "particle in a box" states above the gap. When $V_Z < \Delta$ the spectrum is fully gapped due that the spectrum is dominated by the pairing terms and the system is in the topologically trivial phase.

By increasing the Zeemann energy the gap is decreased and closes around $V_Z = \Delta$ since $\text{E}(V_Z = 0) = \Delta$. This point marks the topological phase transition. When $V_Z > \Delta$ the system is in the topologically non-trivial phase. This is characterized by that there are two states at zero energy, which are separated from the rest of the states by a gap. It should also be noted that these values are in agreement with the theory presented in Section 2.1 where it was shown that the system is in the topologically non-trivial phase when $V_Z > \sqrt{\Delta^2 + \mu^2}$.

Next we consider a nanowire with a length of $2\,\mu$m. The spectrum as function of V_Z is plotted in Fig. 3.1b. From this plot we see that the states at zero energy starts oscillating as a function of increased Zeeman field. This is due to that when the wire is made shorter the MBSs start to overlap. Due to the oscillations of the energies close to zero we denote these *near-zero modes*.

We now investigate what happens when the length of the nanowire is varying. The result is plotted in Fig. 3.1c with the near zero-modes marked in red. The Zeeman energy has been chosen to $V_Z = 0.3\,\text{meV}$ which ensures that $V_Z > \Delta$, thus the system is in the topologically non-trivial phase. When the wire is shorter then $L < 2\,\mu\text{m}$ the near zero modes start oscillating and the smaller L is the larger the amplitude of the oscillations. This reflects that the overlap between MBSs increase as the wire is made shorter. The amplitude of the oscillations decrease as L increase and disappear just before $L = 2\,\mu\text{m}$. Thus we look further into a nanowire with $L = 2\,\mu\text{m}$.

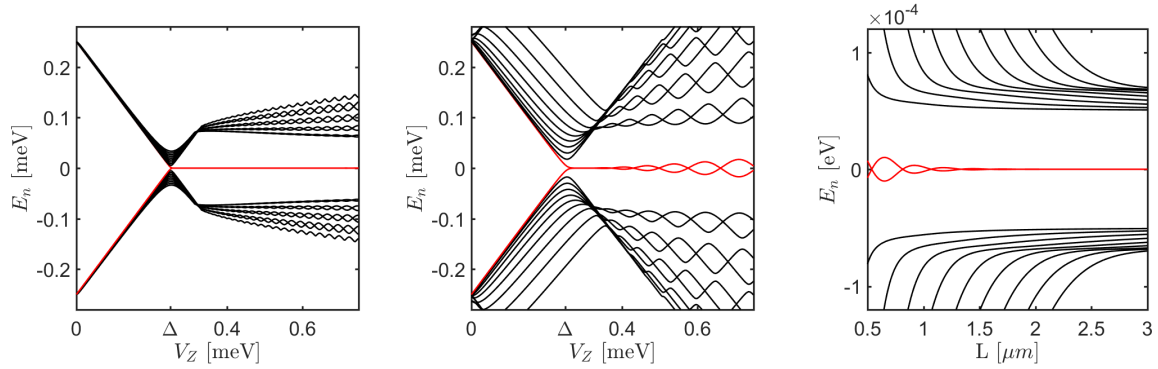

FIG. 3.1. (a) $\{E_n\}$ as function of V_Z for a wire with $L = 7\,\mu\text{m}$. The red curves show $E_{0,1}$ and the black curves show the states above and below $E_{0,1}$. (b) $\{E_n\}$ of the homogeneous nanowire as function of magnetic field, V_Z. $L = 2\,\mu\text{m}$. The red curves correspond to $E_{0,1}$ and the black to above and below lying states. (c) $\{E_n\}$ of nanowire as function of L, $V_Z = 0.3\,\text{meV}$. By decreasing the length of the nanowire the amplitude of the oscillations of the near zero-modes increase.

Figs. 3.2a to 3.2c show the spectrum for a sequence of specific values of the magnetic field and Figs. 3.2d to 3.2f the corresponding probability density for the three lowest states. In Fig. 3.2a the Zeeman field is chosen to $V_Z = 0.15\,\text{meV}$ and thus the system is in the topologically trivial phase. As expected from this the spectrum has a gap around $E = 0$. The corresponding probability densities (Fig. 3.2d) shows similarities with those of a one-dimensional potential well where the wave functions are sinusoidal functions. By increasing the Zeeman field such that the system is in the topologically non-trivial phase ($V_Z > \Delta$) two states, MBSs, are formed at the ends of the wire. These are plotted, for $V_Z = 0.33\,\text{meV}$, in Fig. 3.2e, where the red and blue curves correspond to the probability density of the MBSs. The probability densities for the two first excited states spread over the entire nanowire (green and black curves). Fig. 3.2f shows MBS for $V_Z = 0.43\,\text{meV}$. Due to the increase in magnetic field the probability densities of the MBSs become less localized and spread further into the nanowire compared to when a smaller magnetic field is applied. This agrees with what has been theoretically predicated [25] and is also consistent with that the amplitude of the oscillations in the near-zero modes increase with increasing magnetic field.

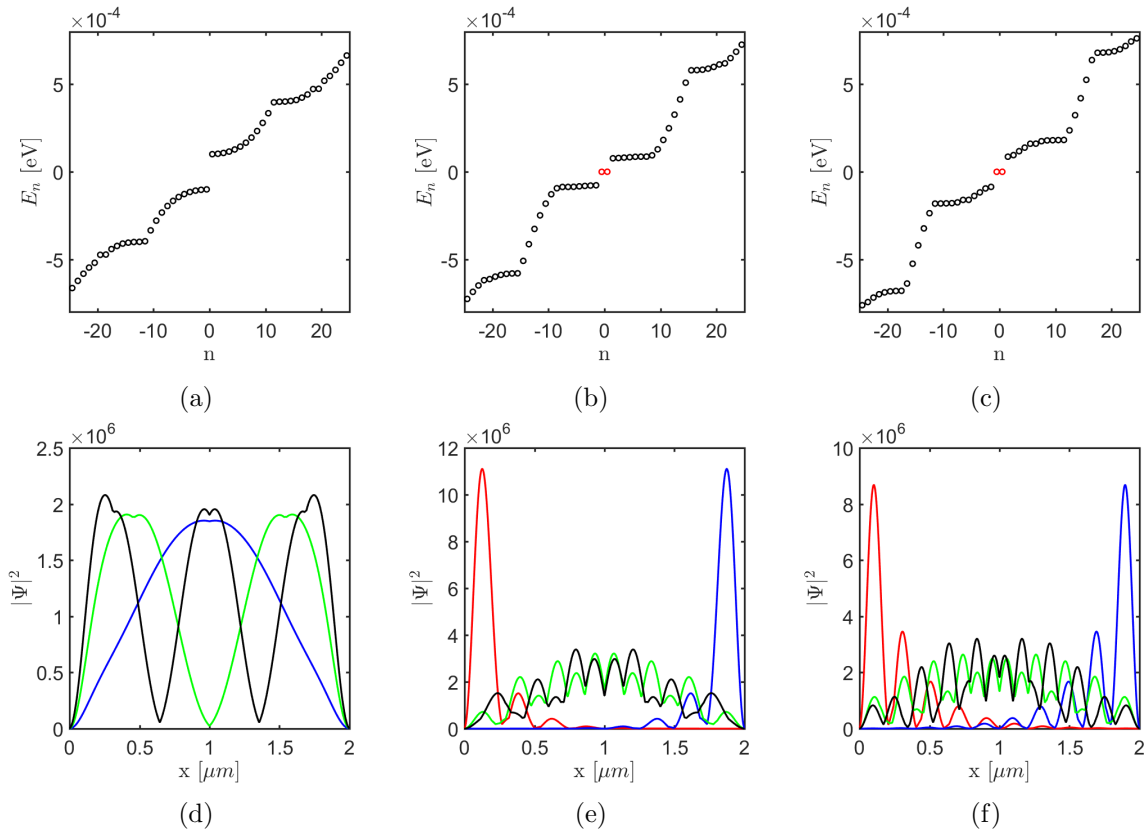

FIG. 3.2. (a) Spectrum (the eigenvalues of Eq. (2.14) closest to zero plotted as a function of eigenvalue number) for $V_Z = 0.15\,\text{meV}$. The corresponding probability density for the three lowest states with positive energy is plotted in (d). (b) Spectrum for $V_Z = 0.33\,\text{meV}$. The near zero modes are marked in red. The probability density of the MBSs and the two first excited states with positive energy are plotted in (e). (c) Spectrum for $V_Z = 0.43\,\text{meV}$ and the probability density of the MBSs and the two first excited states are plotted in (f). (d) $V_Z = 0.15\,\text{meV}$. Blue line correspond to the ground state, green line to the first excited state and black line to the second excited state. (e) Probability densities for $V_Z = 0.33\,\text{meV}$. The red and blue line corresponds each to a MBS. The green and black waves shows the first and second excited state respectively. (f) Probability densities for $V_Z = 0.43\,\text{meV}$.

3.2 Nanowire with potential barriers

In this section we investigate the possibility of decreasing the overlap between the MBSs by inducing a potential change in the nanowire. The potential change is modulated through the term Eq. (2.18) and the modulation will act as potential barriers in the nanowire. The width of the potential barrier(s), $w_{barrier}$, is determined by the lattice constant, a, and the number of sites that are assigned with the value of the height of the barrier, V_0. Three different cases are investigated, all for a nanowire with $L = 2\,\mu$m:

- A nanowire with one potential barrier with $w_{barrier} = 500\,$nm and V_0 varying between 0 and 6 meV.
- A nanowire with one potential barrier with $V_0 = 0.05\,$meV and $w_{barrier}$ varying between 50 and 1500 nm
- A nanowire with $V_0 = 0.05\,$meV, $w_{barrier} = 50\,$nm. The number of barriers in the nanowire, N, varies between 0 and 15.

For every case the ground state energy, E_1 as a function of the magnetic field, V_Z is studied. This is where the main interest lies since this gives information about how the overlap between the near-zero modes is affected and the magnetic field is also one of those parameters that is possible to control during experiments. Due to the particle-hole symmetry it is only necessary to consider the positive states. For quantum computation it is important to have a large gap between the zero-modes and the bulk states since a larger gap gives a better protection against various perturbations. Therefore we investigate both the energy of the first excited state as well as the gap, $E_G = E_2 - E_1$. We also investigate the mean-value of E_1, $\bar{E_1}$, and the mean-value of E_2, $\bar{E_2}$, taken between the point for the phase transition and $V_Z = 3\Delta$. The reason for doing this is that the mean values should give a good indication if the overlap is in general increasing or decreasing. Furthermore, the ratio, $\frac{\bar{E_2}}{\bar{E_1}}$, normalized with $\frac{\bar{E_2}}{\bar{E_1}}\Big|_{V_0=0}$ is studied. This gives an indication whether $\bar{E_1}$ or $\bar{E_2}$ decreases fastest if both are decreasing. A measure of how E_1 reacts to the change of the applied magnetic field is given by

$$\frac{dE_1}{dV_Z}. \tag{3.1}$$

The derivative is investigated since if the derivative is large this implies that a small change in the magnetic field may result in a large energy splitting ($E_1 - E_0$) between the near-zero modes, which means an increase in the overlap between the MBSs. This is important to know for experiments since if the derivative is large then small fluctuations in the magnetic field can suddenly make the MBSs overlap very much.

We also study the probability density of the MBSs to ensure that we have localized states at the ends of the nanowire even when we have a potential barrier in the nanowire. From the probability densities it might also be possible to understand some of the physics we can't understand from just looking at the energy eigenvalues. When investigating the probability densities we choose to do this for a Zeeman field for which the overlap is small and furthermore, we also choose a field for which the overlap is similar to that of MBSs in a nanowire without potential barriers to be able to compare the MBSs of a homogeneous and inhomogeneous nanowire.

3.2.1 Potential barrier with varying height

In this section we consider a nanowire with a potential barrier with $w_{barrier} = 500\,\text{nm}$, which is placed in the middle of the nanowire. The height of the barrier is varied. Fig. 3.3a shows E_1 and E_2 as a function of V_Z for a nanowire without potential barrier and for a nanowire with a potential barrier of different values for V_0.

It is clearly seen that the potential barrier has an effect on the energy eigenvalues. The most noticeable is that E_2 decrease in energy and the larger the barrier is the larger the energy decrease is. Fig. 3.3b shows a zoom in around E_1. From the zoom it is seen that the peaks of the oscillations are shifted to the right and that the amplitude of the oscillations increase. When $V_0 = 0.2\,\text{meV}$ the energy splitting between the near-zero modes become large directly after the point when the system enters the topologically non-trivial phase ($V_Z \approx \Delta$). The near-zero modes also show more oscillations compared to when there is no potential barrier in the nanowire. However, there is a decrease in the overlap around $V_Z = 0.4\,\text{meV}$ of about a half and the peak around $V_Z = 0.6\,\text{meV}$ is not increasing compared to the last peak.

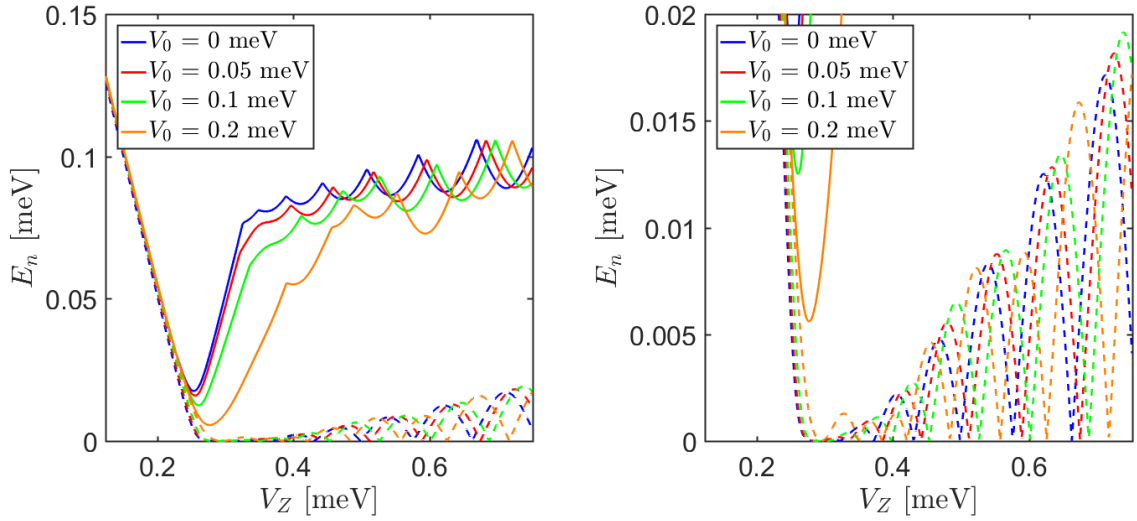

FIG. 3.3. (a) E_1 (dashed line) and E_2 (solid line) as function of V_Z for a nanowire with a potential barrier with height V_0 and width, $w_{barrier} = 500\,\text{nm}$. (b) Zoom in around E_1.

The derivative, dE_1/dV_Z, Fig. 3.4a mainly confirms that the oscillation peaks are shifted when increasing the barrier height. In addition it shows that a nanowire with a larger barrier, in this case $V_0 = 0.2\,\text{meV}$, is more affected by a small change in V_Z for small Zeeman fields. In Fig. 3.4b, E_G is plotted. This merely confirms that E_2 moves towards E_1 as V_0 becomes larger.

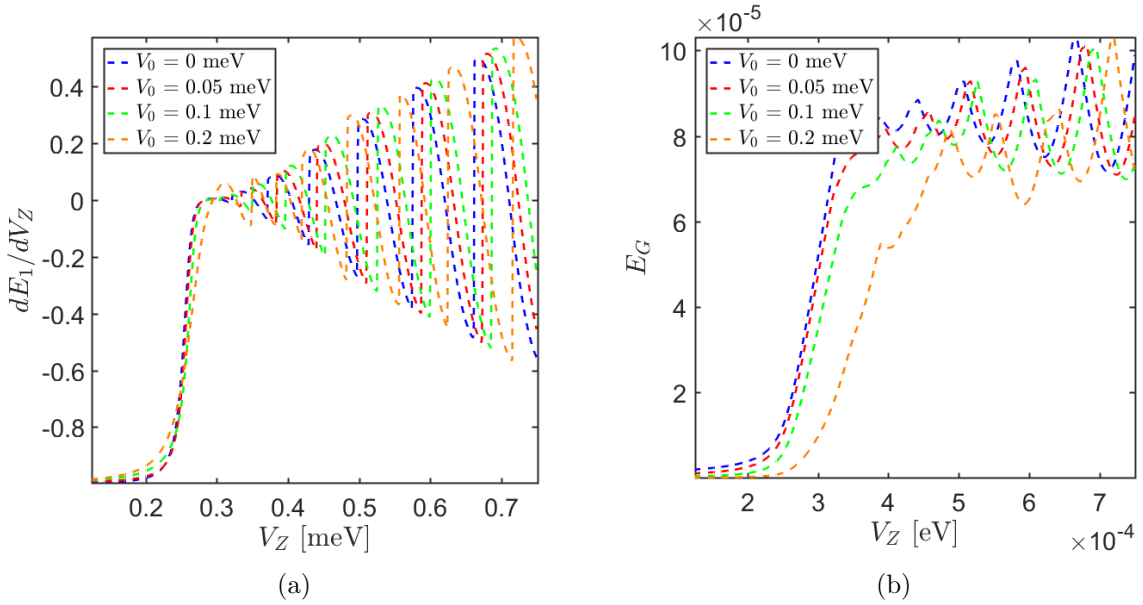

(a) (b)

FIG. 3.4. (a) dE_1/dV_Z as function of V_Z. (b) E_G as a function of V_Z. For both plots, $w_{barrier} = 500\,\text{nm}$.

Figs. 3.5a to 3.5c show $\bar{E}_1$, $\bar{E}_2$ and $\frac{\bar{E}_2}{\bar{E}_1}$ normalized with $\frac{\bar{E}_2}{\bar{E}_1}\Big|_{V_0=0}$ as a function of V_0. For V_0 smaller than approximately 0.08 meV there is a slight increase in $\bar{E}_1$. When V_0 is between 0.1 to 0.2 meV there is a decrease in $\bar{E}_1$. For barrier heights above 0.2 meV the mean energy is monotonously increasing, which indicates a decrease in the energy splitting between the near-zero modes. The ratio, $\frac{\bar{E}_2}{\bar{E}_1}$ is decreasing no matter the barrier height. This indicates that, in the interval where $V_Z \in [0.080.2]\,\text{meV}$ and $\bar{E}_1$ is also decreasing, E_2 is affected more by the barrier than E_1 is.

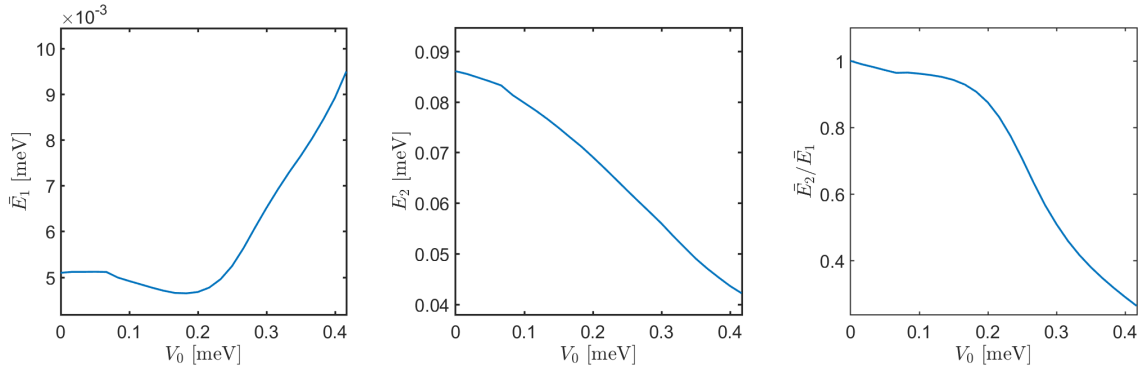

(a) (b) (c)

FIG. 3.5. (a) $\bar{E}_1$ as function of barrier height. (b) $\bar{E}_2$ as function of barrier height. (c) $\frac{\bar{E}_2}{\bar{E}_1}$ as function of barrier height normalized with $\frac{\bar{E}_2}{\bar{E}_1}\Big|_{V_0=0}$.

The probability density of the MBSs for different barrier heights are shown in Figs. 3.6a to 3.6c and a zoom in aroundthe middle of the nanowire is shown in Fig. 3.7. A small barrier, $V_0 = 0.05\,\text{meV}$ (Fig. 3.6b), shows a small shift between the MBSs and there is a smaller overlap between them compared to having no barrier (Fig. 3.6a). A larger barrier (Fig. 3.6c) shows an even smaller overlap between the MBSs. However, the weight of the MBSs for the case of $V_0 = 0.2\,\text{meV}$ seems to be shifted more towards the middle of the nanowire.

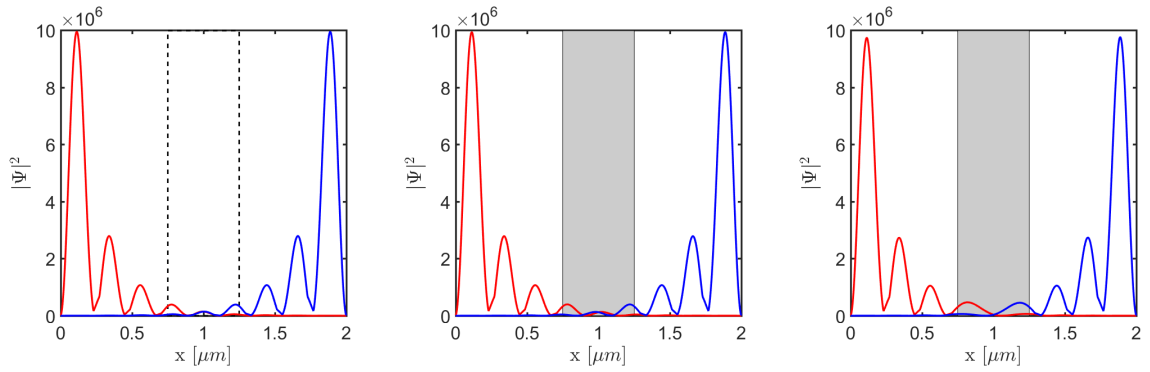

FIG. 3.6. The weight of MBSs for (a) nanowire with no potential barrier, (b) for a nanowire with a potential barrier, $V_0 = 0.05meV$ and (c) for a nanowire with potential barrier, $V_0 = 0.2\,\text{meV}$. $V_Z = 0.3781\,\text{meV}$ for all plots. The grey area in the plots indicates the location of the potential barrier

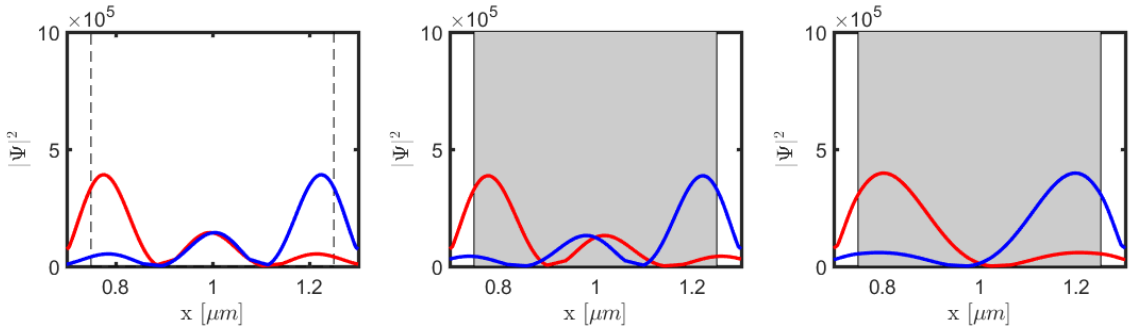

FIG. 3.7. (Left panel) Zoom in of Fig. 3.6a around the middle of the nanowire. (Middle panel) Zoom in of Fig. 3.6b around the middle of the nanowire. (Right panel) Zoom in of Fig. 3.6c around the middle of the nanowire. The gray area in the plots indicates the location potential barrier.

From Fig. 3.5a it was seen that $\bar{E_1}$ is increasing monotonously. To understand why this is, we investigate what happens when making the amplitude of the barrier large. Figs. 3.8a and 3.8b shows the four smallest states with positive energy for a nanowire with a potential barrier as function of V_Z. V_0 varies between Δ and $24 \cdot \Delta$. When increasing the barrier height, E_2 approaches E_1 as seen in Fig. 3.3a. For barrier heights around Δ (Fig. 3.8a), $E_G = 0\,\text{eV}$ and E_1 and E_2 are degenerate. The degeneracy is due to that the barrier makes the nanowire act as two systems, each side of the barrier hosts a pair of MBSs. Fig. 3.9a shows the spectrum when $V_0 = 1\,\text{meV}$ and $V_Z = 0.44\,\text{meV}$. The states above the near zero-modes are also degenerate but the degeneracy is broken for states with energy above $0.5\,\text{meV}$. This is due to the increased coupling between states on the different sides of the barrier, which has an energy that approaches the height of the barrier. A consequence of the degeneracy is that the MBSs are now written as a linear combination of the four states closest to zero,

$$\Psi = a\psi_1 + b\psi_0 + c\psi_2 + d\psi_{-1}, \tag{3.2}$$

where $a, b, c, d \in \mathbb{R}$. The probability density of the MBSs are plotted in Fig. 3.9b. This confirms that the nanowire is effectively split in two since each part host a pair of MBSs. Further investigations of Fig. 3.8 shows that the degeneracy of the near-zero modes are broken by increasing the magnetic field. It is seen from Figs. 3.8a and 3.8b that the larger the barrier is the larger the

magnetic field has to be to break the degeneracy. When $V_0 = 1\,\text{meV}$ the magnetic field required to break the degeneracy is larger than the magnetic field strengths that lies in the chosen interval.

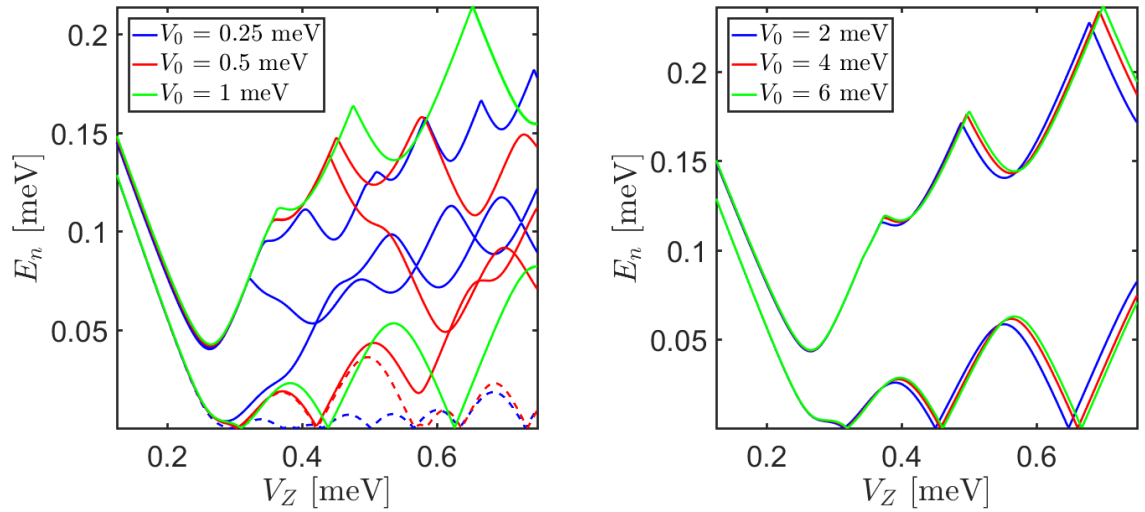

(a) (b)

FIG. 3.8. E_n, $n \in \{1, 2, 3, 4\}$ as a function of V_Z for barriers with $V_0 \geq \Delta$, (a) shows E_n for medium height barriers. (b) Shows E_n for large barriers.

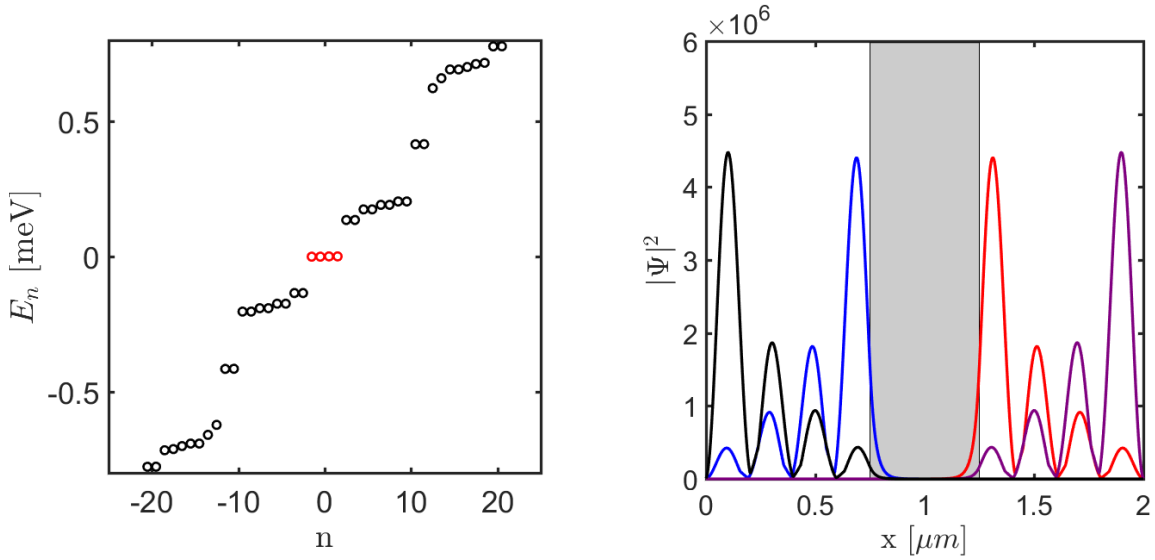

(a) (b)

FIG. 3.9. (a) Energy spectrum for nanowire with a potential barrier with $w_{barrier} = 500\,\text{nm}$ and $V_0 = 1\,\text{meV}$. $V_Z = 0.44\,\text{meV}$. (b) The probability density of the MBSs. The wave functions is now given by Eq. (3.2) and in this case $\Psi_1 = \psi_1 - \psi_0^\dagger + \psi_2 - \psi_{-1}^\dagger$ (red), $\Psi_2 = \psi_1 + \psi_0^\dagger - \psi_2 - \psi_{-1}^\dagger$ (blue), $\Psi_3 = \psi_1 + \psi_0^\dagger + \psi_2 + \psi_{-1}^\dagger$ (black), $\Psi_4 = \psi_1 - \psi_0^\dagger - \psi_2 + \psi_{-1}^\dagger$ (purple). The gray area indicates the location of the barrier.

These results show that by tuning the height of the barrier a decrease in the overlap between the MBSs, even though it is small, can be obtained. Furthermore, by making the barrier height

large, the nanowire can effectively be split into two systems. However, when increasing the height of the barrier E_G is always made smaller.

3.2.2 Potential barrier with varying width

In this section we consider a nanowire with a potential barrier with varying width, $w_{barrier}$. In Fig. 3.10a E_1 and E_2 are plotted as a function of V_Z and Fig. 3.10b shows a zoom in around E_1. The main effect of increasing the barrier width is that the oscillations in E_0 are shifted towards larger Zeeman energy. The peak-amplitudes, however, change irregularly. This is e.g. seen for the barrier with $w_{barrier} = 500\,\text{nm}$. When $V_Z \approx 0.56\,\text{meV}$ the peak is shifted and has a larger amplitude compared to the case of no barrier. However when $V_Z \approx 0.62\,\text{meV}$ the peak is merely shifted.

The mean values of E_1 and E_2 and the mean of their ratio are shown in Figs. 3.11a to 3.11c. $\bar{E}_1$ shows no significant change for barriers with $w_{barrier} < 1000\,\text{nm}$. When the barrier is wider than 1000 nm, $\bar{E}_1$ shows a decrease with increased barrier width. This shows that there in general is a decrease in the overlap between the MBSs, which is in this case hard to see by just looking at $E_1(V_Z)$. From both Fig. 3.10a and Fig. 3.11b it is clear that by making the barrier wider E_2 is decreasing. When $w_{barrier} < 1000\,\text{nm}$ the decrease in E_2 is larger than the decrease in E_1 as seen from Fig. 3.11c and there is a negative effect on E_G. By increasing the width such that $w_{barrier} > 1000\,\text{nm}$, the ratio $\frac{\bar{E}_2}{\bar{E}_1}$ normalized with $\frac{\bar{E}_2}{\bar{E}_1}\Big|_{V_0=0}$ is increasing and thus E_G is increasing.

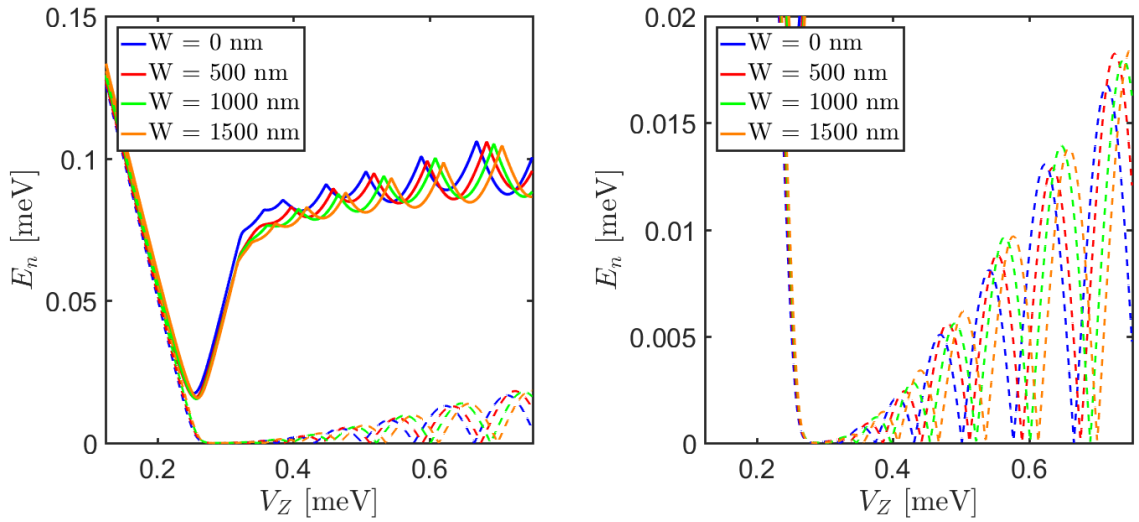

FIG. 3.10. (a) E_1 (dashed line) and E_2 (solid line) as function of V_Z. (b) Zoom-in around E_1.

The probability density of the MBSs in a nanowire without a potential barrier and in a nanowire with a potential barrier with $w_{barrier} = 1500\,\text{nm}$ is plotted in Figs. 3.12a and 3.12b. The magnetic field is $V_Z = 0.518\,\text{meV}$. The data cursor indicates that there is a significant decrease in in the amplitude of the MBSs in the middle of the nanowire when the potential barrier is present. Moreover there is a shift in the oscillation peaks indicating a smaller overlap between the wave functions.

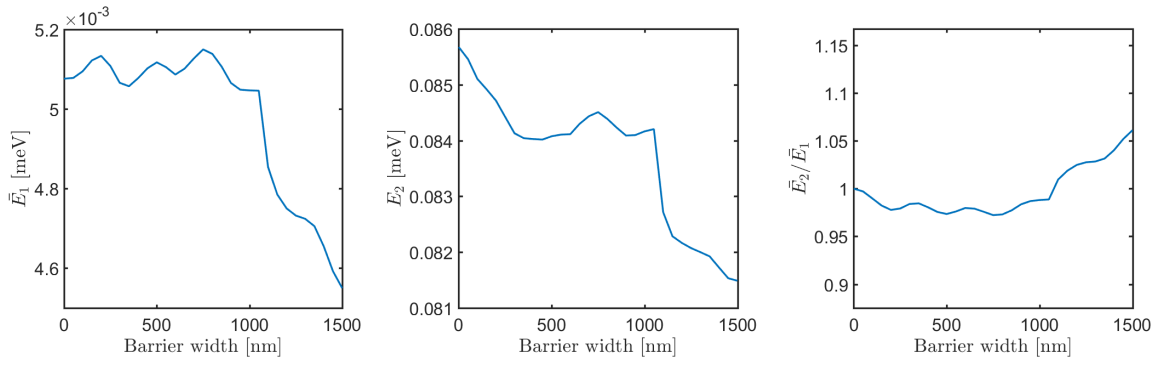

(a) (b) (c)

FIG. 3.11. (a) $\bar{E}_1$ as function of $w_{barrier}$. (b) $\bar{E}_2$ as function of $w_{barrier}$. (c) $\frac{\bar{E}_2}{\bar{E}_1}$ normalized with $\frac{\bar{E}_2}{\bar{E}_1}\Big|_{V_0=0}$ as function of $w_{barrier}$.

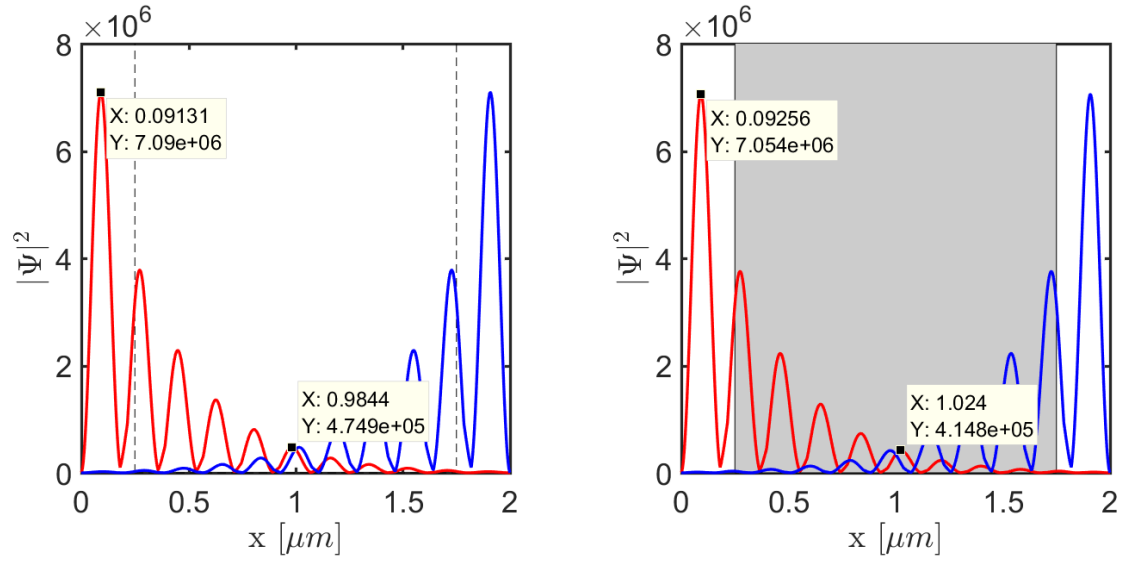

(a) (b)

FIG. 3.12. Probability density of the MBSs for (a) nanowire without potential barrier and (b) for a nanowire with a potential barrier. $V_0 = 0.05\,\text{meV}$ and $w_{barrier} = 1500\,\text{nm}$. The gray area indicate the barrier. For both plots $V_Z = 0.518\,\text{meV}$.

3.2.3 Varying number of potential barriers

In this section we consider the third case, a nanowire with a varying number of potential barriers. In Fig. 3.13a E_1 and E_2, of a wire with a varying number of potential barriers, as a function of V_Z are plotted, and Fig. 3.13b shows a zoom-in around E_1. The mean values of these as well as the ratio of the mean values are plotted in Figs. 3.14a to 3.14c. The height and the width of the barriers are $V_0 = 0.05\,\text{meV}$ and $w_{barrier} = 50\,\text{nm}$ respectively. From the mean values it is clearly seen that the largest deviations from a homogeneous nanowire are for a nanowire with either six or thirteen potential barriers. In both cases the mean energy is decreasing. However, the ratio is increasing, which indicates that the decrease in E_1 should be stronger than the decrease in E_2. The decrease in $\bar{E}_1$ for the case of six and thirteen potential barriers is due to the decrease in E_1 for a Zeeman energy around $V_Z = 0.7\,\text{meV}$. Apart from this, the peaks in the oscillations of E_1 are increasing compared to the case of a homogeneous

nanowire. From $\bar{E}_1$ (Fig. 3.14a) it is seen that when there are ten potential barriers in the nanowire the mean of the overlap is increasing. The increase in the mean for ten barriers is mainly due to the larger increase in E_1 around $V_Z = 0.55\,\text{meV}$ (Fig. 3.13b). For ten barriers there is also a decrease in the overlap of the MBSs for $V_Z \approx 0.47\,\text{meV}$. The overlap is about a third of the overlap for the homogeneous nanowire. This analysis shows that it might be possible to "tune" the barriers such that the overlap is small in a narrow interval of the magnetic field.

The probability density of the MBSs in a homogeneous nanowire and in a nanowire with ten potential barriers is plotted in Figs. 3.15a and 3.15b. For both plots $V_Z = 0.5\,\text{meV}$. As seen from the data cursors the weight of the MBSs is shifted towards the the ends of the nanowire with ten potential barriers compared to the homogeneous nanowire.

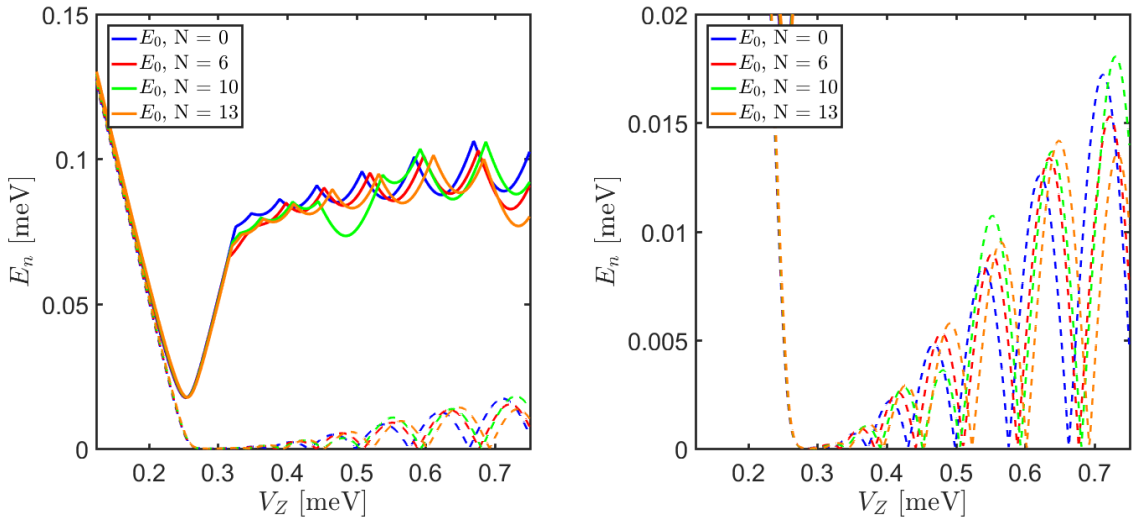

FIG. 3.13. (a) E_1 (dashed line) and E_2 (solid line) as function of V_Z. (b) Zoom-in around E_1.

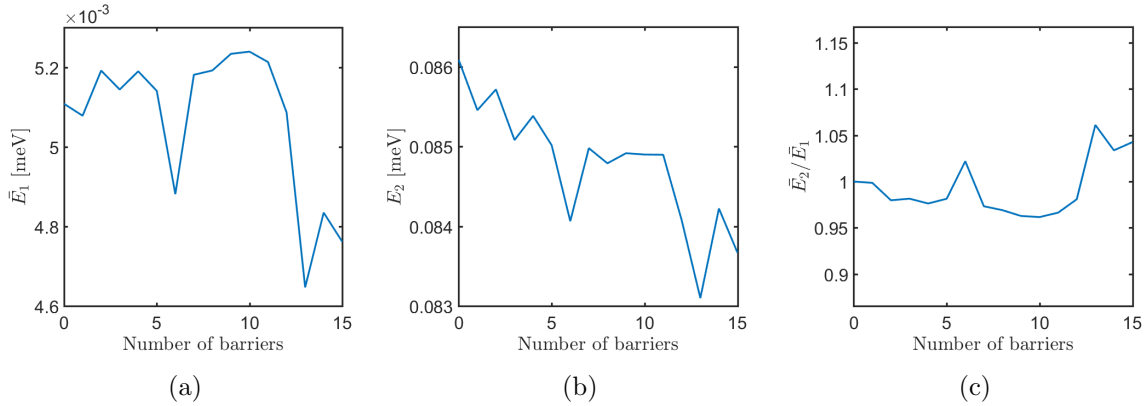

FIG. 3.14. (a) $\bar{E}_1$ as function of number of barriers. (b) $\bar{E}_2$ as function of number of barriers. (c) $\bar{E}_2/\bar{E}_1$ normalized with $\frac{\bar{E}_2}{\bar{E}_1}\Big|_{V_0=0}$ as function of number of barriers.

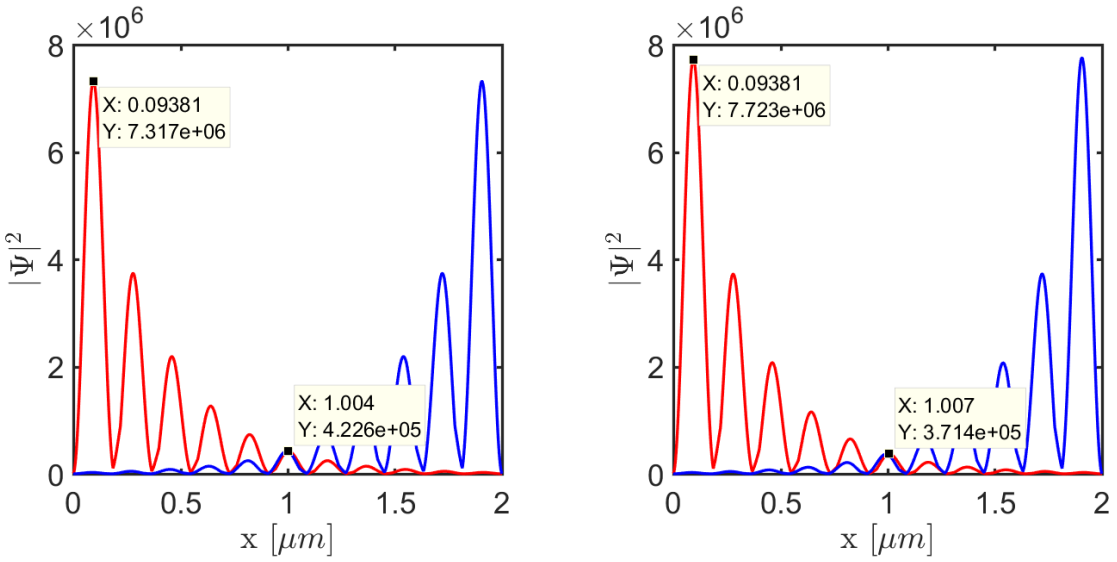

(a) (b)

FIG. 3.15. (a) The weight of the MBSs for (a) a homogeneous nanowire and (b) a nanowire with ten potential barriers. $V_Z = 0.5\,\text{meV}$ for both cases.

3.3 Superlattice

The results from the nanowire with potential barriers shows that there is indeed a possibility to decrease the overlap between the MBSs. Having just one potential barrier shows that in a certain range of V_0, there is a decrease in the overlap between the MBSs, see Fig. 3.3b. The third case, a nanowire with a varying number of potential barriers shows that by increasing the number of barriers there is, for certain Zeeman fields, a decrease in the overlap as well, see Fig. 3.13b. This leads one to think that being able to increase the number of barriers in the wire as well as the height of the barriers may lead to an even smaller overlap between the MBSs. A way to achieve such a structure is by using a superlattice structure. A superlattice is a structure of different materials layered on top of each other in a periodic way. The difference between the superlattice and the nanowire with many potential barriers is that the barriers in the superlattice are much thinner and the height much larger, which results in that mini-bands form in the structure.

The Kronig-Penny model is a simplified model to describe an electron in a one-dimensional periodic potential structure. The Kronig-Penney structure is shown in Fig. 3.16a.

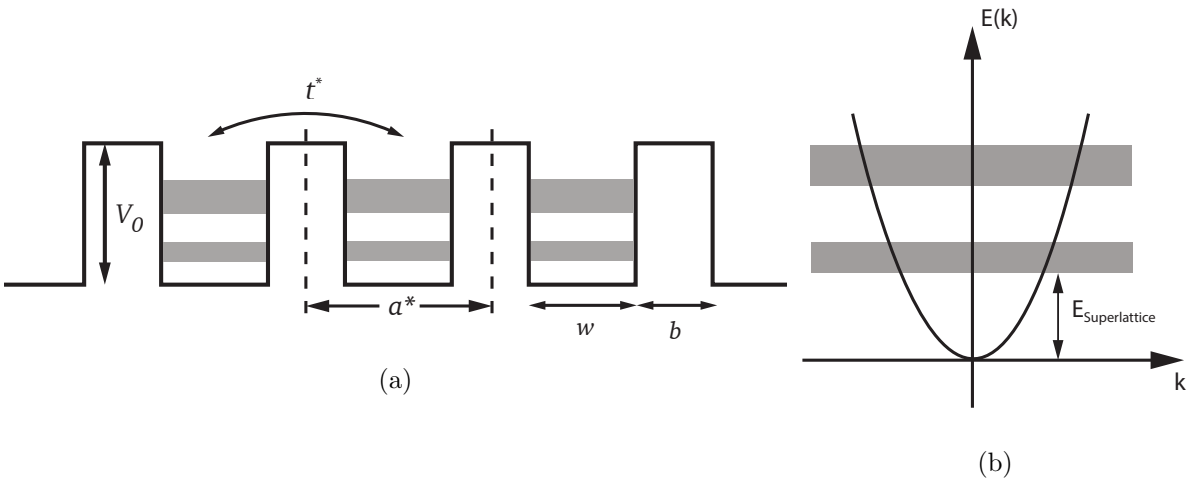

(a) (b)

FIG. 3.16. (a) Kronig-Penny model for a one-dimensional periodic potential structure. V_0 is the height of the superlattice barriers, w is the distance between two barriers and b is the width of a barrier. a^* defines a lattice cell of the potential structure and t^* is the effective hopping parameter of the superlattice. The grey areas indicate the mini-bands. (b) The allowed energies of the superlattice (mini-bands shown in grey) compared to the free electron parabola. $E_{Superlattice}$ defines the smallest allowed energy in the superlattice.

The Kronig-Penny model is solved in [24], with $m^*(k) = m^*$, and it is found that

$$\cos(ka^*) = \cos(k_1 a^*) + \frac{m^* \cdot a^* \cdot b \cdot V_0}{\hbar^2} \cdot \frac{sin(k_1 a^*)}{k_1 a^*} \tag{3.3}$$

where k is the effective wave vector of the structure, m^* is the effective mass, V_0 is the barrier height, b the barrier width and a^* is the lattice constant and defines a lattice cell of the superlattice as indicated in Fig. 3.16a. The wave function in each cell is then described by the wave number k_1 and the energy is given by $E = \hbar^2 k_1^2 / 2m^*$. Combining $E = \hbar^2 k_1^2 / 2m^*$ and Eq. (3.3) gives the energy as a function of the wave number k. E as function of k is plotted in Fig. 3.17 for three different cases. The different cases show how the mini-bands are affected when changing either a^* or the product $b \cdot V_0$.

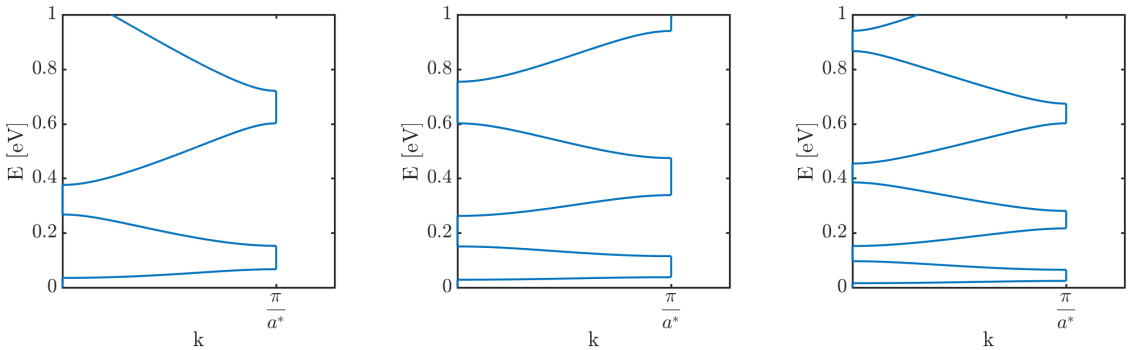

FIG. 3.17. Energy as a function of k for different settings of a^* and b. V_0 is fixed at 0.2 eV. (a) $a^* = 15$ nm and $b = 5$ nm, (b) $a^* = 20$ nm and $b = 10$ nm, (c) $a^* = 25$ nm and $b = 5$ nm. Note that the band start at $E = 0$.

The superlattice is modelled in the same way as the potential barriers. Due to the minibands that form in the superlattice the bottom of the band does not correspond to $E = -2t$. To take this into account μ is chosen such that $\mu = -2t_0 + E_{Superlattice}$ where $E_{Superlattice}$ is the energy of the bottom of the lowest lying miniband in the superlattice (see Fig. 3.16b).

Fig. 3.18a shows E_1 and E_2 as a function of V_Z for a nanowire without superlattice and for a nanowire with superlattice with different amplitudes for V_0. The superlattice has $a^* = 15\,\text{nm}$ and $b = 5\,\text{nm}$. As seen E_2 decrease in energy over the whole interval and the decrease increases with increasing V_0. This is also supported in Fig. 3.19b, which shows that $\bar{E_2}$ is decreasing as function of increasing V_0. A closer analysis of E_1 shows that there is no systematic change in $E_1(V_Z)$ when changing V_0. Fig. 3.19a shows $\bar{E_1}$ as function of V_0. From this we see that there is a general decrease in the overlap compared to the homogeneous nanowire. $\bar{E_1}$ is however not monotonically decreasing when increasing V_0 which is due to the non-systematic change in E_1 (Fig. 3.18b). When $V_0 = 160\,\text{meV}$ the peaks of the oscillations for E_1, for $V_Z < 0.6\,\text{meV}$, are mostly centred beneath the peaks of E_1 for a homogeneous nanowire (Fig. 3.18b). The amplitude of the peaks for the superlattice are all smaller than those of a homogeneous nanowire which shows that, even though the effect is small, it is possible to make the overlap smaller for all values of V_Z in the chosen interval.

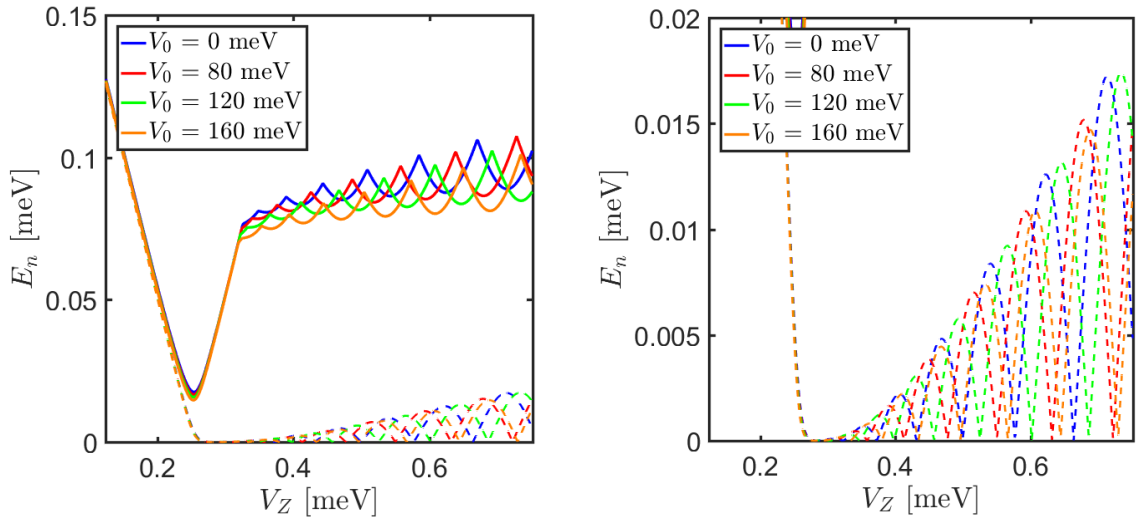

FIG. 3.18. (a) E_1 (dashed line) and E_2 (solid line) as function of V_Z (b) Zoom in of (a) around E_1.

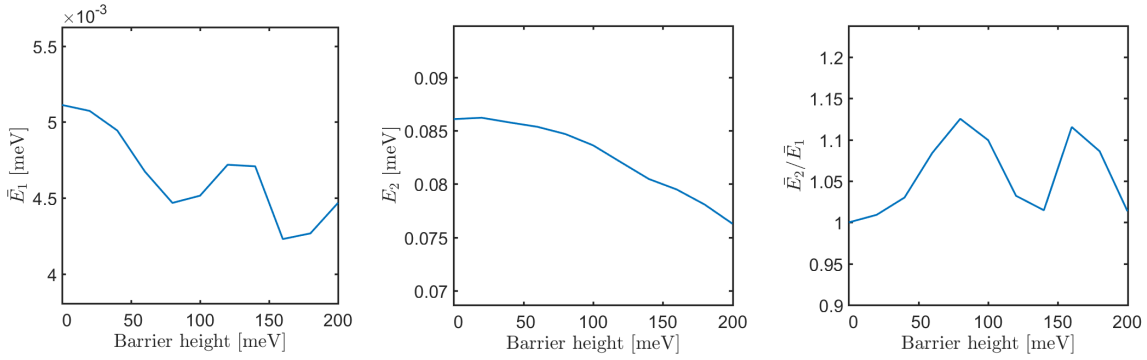

(a) (b) (c)

FIG. 3.19. (a) $\bar{E}_1$ as function of V_0. (b) $\bar{E}_2$ as function of V_0. (c) $\frac{\bar{E}_2}{\bar{E}_1} \cdot (\frac{\bar{E}_1}{\bar{E}_2}\Big|_{V_0=0})$ as function of V_0.

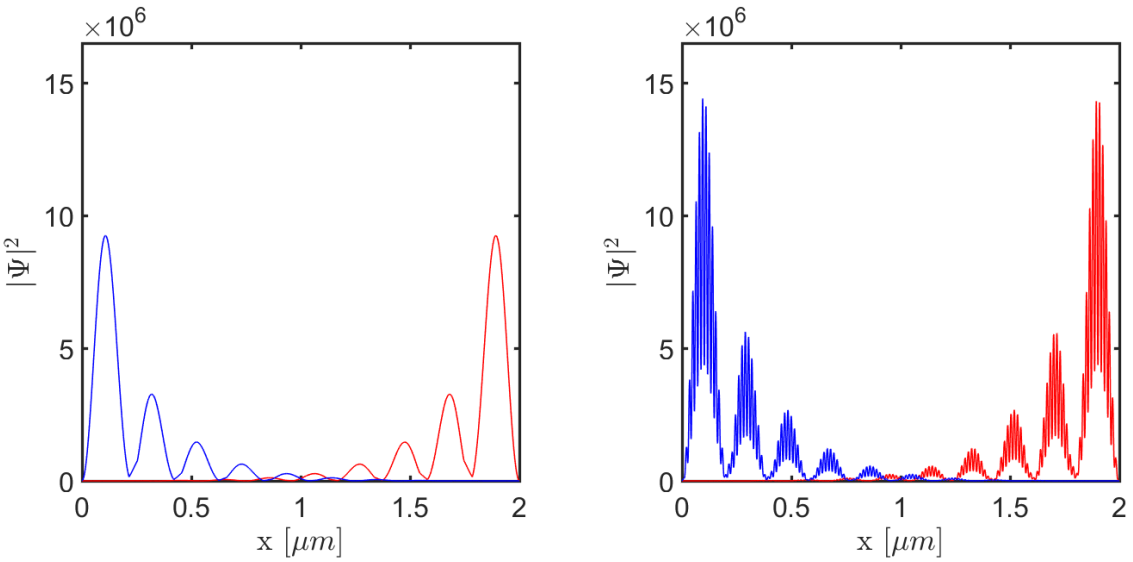

(a) (b)

FIG. 3.20. The weight of the MBSs in (a) a homogeneous nanowire and (b) a nanowire with a superlattice, $V_0 = 160\,\text{eV}$. For both cases $V_Z = 0.408\,\text{meV}$

.

The weight of the MBSs in a homogeneous nanowire and in a nanowire with superlattice is plotted in Fig. 3.20. A close analysis show that there is a small shift of the MBSs towards the ends of the nanowire, in the case of the nanowire with superlattice, which indicates a decrease in the overlap of the MBSs. Also noticeable from the MBSs of the nanowire with superlattice is the strong oscillations. The oscillations can be explained by considering the momentum operator,

$$\hat{p} = -i\hbar\frac{\partial}{\partial x} \tag{3.4}$$

and the free electron parabola, Fig. 3.16b. If we consider the expectation value of the square of the momentum operator, $\langle p^2 \rangle$, this should be larger for the wave function of the MBSs in the superlattice than in the homogeneous nanowire due to the large oscillations. This is consistent

with that the chemical potential has to be shifted to larger momentum due to the superlattice. Thus the oscillations in the wave function is due to the increase in momentum.

3.4 Disorder

3.4.1 Disorder in homogeneous nanowire

In reality semiconducting nanowires are never free from impurities and and other defects causing disorder in the nanowire. An infinite wire is topologically protected from all kinds of disorder as long as the gap is not closed. However, since this does not apply to a nanowire that is finite it is also of interest to investigate how nanowires with potential barrier(s) or a superlattice structure react to disorder compared to a homogeneous nanowire. We consider disorder in the potential, which is included by adding a random change to the potential on every lattice site. The disorder is described by the term

$$H_{Disorder} = \sum_i D_i c_{i\sigma}^\dagger c_{i\sigma} \tag{3.5}$$

where D_i is the strength of the disorder on lattice site i. D_i is chosen from a normal distribution $\mathcal{N}(\mu, \sigma)$, where μ is the mean and is set to zero. σ is the standard deviation of the normal distribution and is used to control the strength of the disorder. Since disorder is distributed randomly there will never be two nanowires with the same disorder profile. To take this into account we run a hundred simulations and consider the average of this as well as specific cases. We do simulations for disorder strength varying between 0.1Δ and 2Δ. In this section it should also be noted that a homogeneous nanowire refers to a nanowire that is homogeneous without disorder and a inhomogeneous nanowire refers to a nanowire that has a defined inhomogeneity that is not caused by the disorder.

Fig. 3.21 shows the mean value of E_1 and E_2, after a hundred simulations have been carried out, as a function of V_Z. The nanowire is homogeneous and is subject to disorder in the potential with varying strength. From this plot it is seen that the disorder has the effect of decreasing E_2 while the largest effect it has on E_1 is seen around the points where the near zero-modes are degenerate, which are shifted away from zero energy. When the disorder strength is large (standard deviation $\gtrsim \Delta$) the near-zero mode oscillations disappear as well.

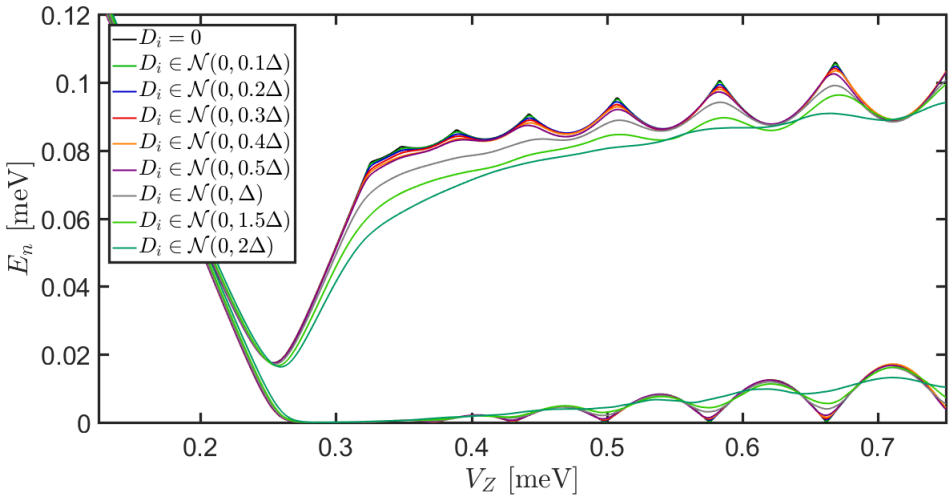

FIG. 3.21. The mean value of E_1 and E_2 as a function of V_Z for a hundred simulations. The nanowire is homogeneous and subject to disorder in the potential with varying strength.

Specific cases for weak disorder are plotted in Fig. 3.22a. To distinguish between states that are subjected to disorder and those that are not, we define $E_{n,Disorder}$ as the states which are subjected to disorder. For small disorder strength the difference between E_1 and $E_{1,Disorder}$ is very small. When the disorder strength becomes larger, in this case $D_i \in \mathcal{N}(0, 0.5\Delta)$, the effect of the disorder is noticeable, which is seen from the increase in the difference between E_1 and $E_{1,Disorder}$. Furthermore, it is due to the random shifts that we see an increase around the points where the near-zero modes are degenerate when considering the mean value of many simulations (Fig. 3.21), and the larger the difference between E_1 and $E_{1,Disorder}$ is the larger the shift is at the points of degeneracy in the mean value (Fig. 3.21). Because of this it is possible to say if the difference $|E_1$ - $E_{1,Disorder}|$ is going to be small or large by just looking at what happens with the mean value of many simulations.

The probability density of the MBSs for a homogeneous nanowire are plotted in Fig. 3.22b. The dashed lines show the MBSs for a nanowire without disorder and these states are symmetric around the middle of the nanowire. The solid lines show the MBSs for a nanowire with disorder. As seen, due to the disorder, the MBS are no longer symmetric. A specific case of strong disorder is plotted in Fig. 3.23a. Due to the strong disorder $E_{n,Disorder}$ differs, to a large extent, from E_n. We see that the amplitude of the near-zero modes may become much larger compared to a nanowire without disorder, which indicate that the overlap is increasing. There, however, still exist points where the energy is zero. A general decrease in the excited state can be seen, which results in a decrease of E_G.

The probability density of the MBSs for a nanowire with strong disorder, $\mathcal{N}(0, 2\Delta)$, is plotted in Fig. 3.23b. Compared to the case of small disorder the MBSs now show a large asymmetry. Moreover, one of the MBSs has become less localized and has its weight shifted towards the middle of the wire. Due to that the MBS has shifted more towards the middle this implies an increase in the overlap between the two MBSs. Furthermore, if either of the MBSs leave the end of the wire the fermionic state consisting of the two MBSs will become less delocalized and sensitive to decoherence.

The reason for the possible change in the overlap due to the disorder is that the disorder induces

an asymmetry in the potential. The asymmetry in the potential leads to that the mixture of spin-up and spin-down states for positive and negative k will be different and due to this the MBSs will be less localized to the edge of the nanowire, which leads to a larger overlap.

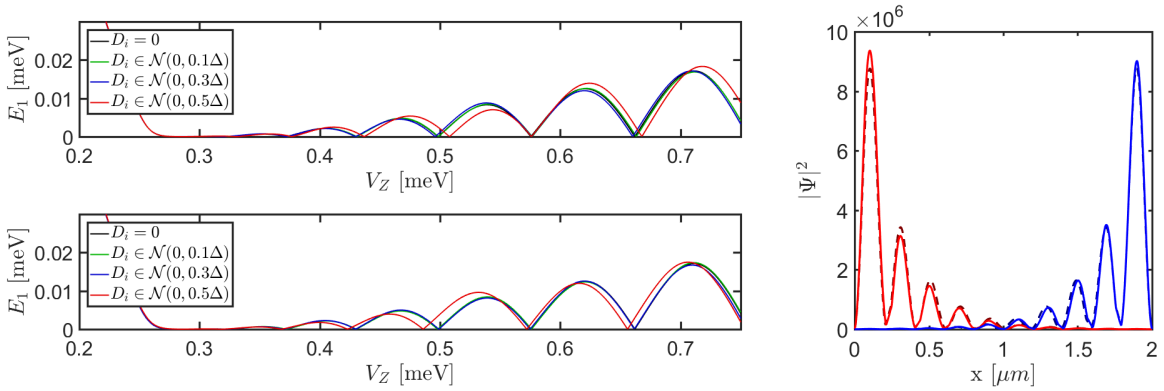

(a) (b)

FIG. 3.22. (a) E_1 as a function of V_Z for a homogeneous nanowire subject to disorder with varying strength. Due to randomness in the disorder the top panel and the bottom panel show different results. (b) Weight of the MBSs for a homogeneous nanowire with disorder (solid lines) and without disorder (dashed lines). $D_i \in \mathcal{N}(0, 0.5\Delta)$ and $V_Z = 0.4266\,\text{meV}$.

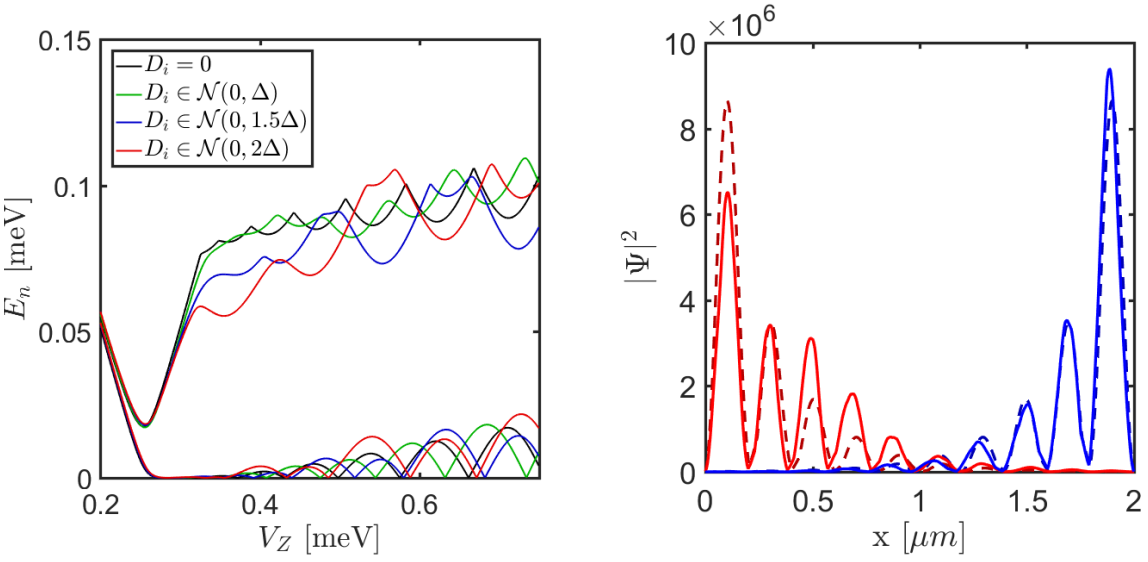

(a) (b)

FIG. 3.23. (a) E_1 and E_2 as a function of V_Z for a nanowire with strong disorder and (b) the weight of the MBSs for a homogeneous nanowire with disorder (solid lines) and without disorder (dashed lines). $D_i \in \mathcal{N}(0, 2\Delta)$ and $V_Z = 0.432\,\text{meV}$.

3.4.2 Disorder in inhomogeneous nanowires

In this section we consider disorder in an inhomogeneous nanowire and compare it to both the case when the nanowire is free from disorder as well as the case of the homogeneous nanowire. From Section 3.4.1 it was seen that the effects of the disorder can be seen from how the energy changes around points where the near-zero modes are degenerate. Thus the change in energy

at the points where the near-zero modes are degenerate is investigated. The change in energy around the points where the near-zero modes are degenerate is $E_{1,Disorder} - E_1$. This energy difference is plotted in Fig. 3.24 for four different cases. The top left panel shows $E_{1,Disorder} - E_1$ for a homogeneous nanowire. The bottom left panel shows $E_{1,Disorder} - E_1$ for a nanowire with a potential barrier with $w_{barrier} = 500\,\text{nm}$ and $V_0 = 0.2\,\text{meV}$. In comparison to the homogeneous nanowire the only significant difference is when $D_i \in \mathcal{N}(0, 2\Delta)$ and V_Z is large. In this case the nanowire is less affected by disorder compared to the homogeneous nanowire.

The top right panel of Fig. 3.24 shows $E_{1,Disorder} - E_1$ for a nanowire with thirteen barriers where $w_{barrier} = 50\,\text{nm}$ and $V_0 = 0.05\,\text{meV}$. For weak disorder the inhomogeneous nanowire is again affected similarly by disorder compared to the homogeneous nanowire. However, for disorder strength of $D_i \in \mathcal{N}(0, \Delta)$ and $D_i \in \mathcal{N}(0, 1.5\Delta)$ the nanowire with thirteen potential barriers is more affected by the disorder then all of the other cases. Furthermore, the effect is almost the same for when $D_i \in \mathcal{N}(0, \Delta)$ and $D_i \in \mathcal{N}(0, 1.5\Delta)$. This indicates that a larger number of simulations should actually be done. However, this was not possible to conduct due to the time limit of this project.

The bottom right panel shows a $E_{1,Disorder} - E_1$ for a nanowire with a superlattice. As for the case of a nanowire with either one or thirteen potential barriers, the nanowire with superlattice shows similar behaviour compared to the homogeneous nanowire for weak disorder. For the largest disorder strength chosen ($D_i \in \mathcal{N}(0, 2\Delta)$) there is a decrease in $E_{1,Disorder} - E_1$ compared to the homogeneous nanowire. The decrease is, however, not stronger than that of the nanowire with one potential barrier. It should be noted from all the plots that the difference, $E_{1,Disorder} - E_1$ is slightly shifted in V_Z. This is due to that, as explained in Section 3.2, points where the near-zero modes are degenerate are shifted for an inhomogeneous nanowire compared to a homogeneous nanowire.

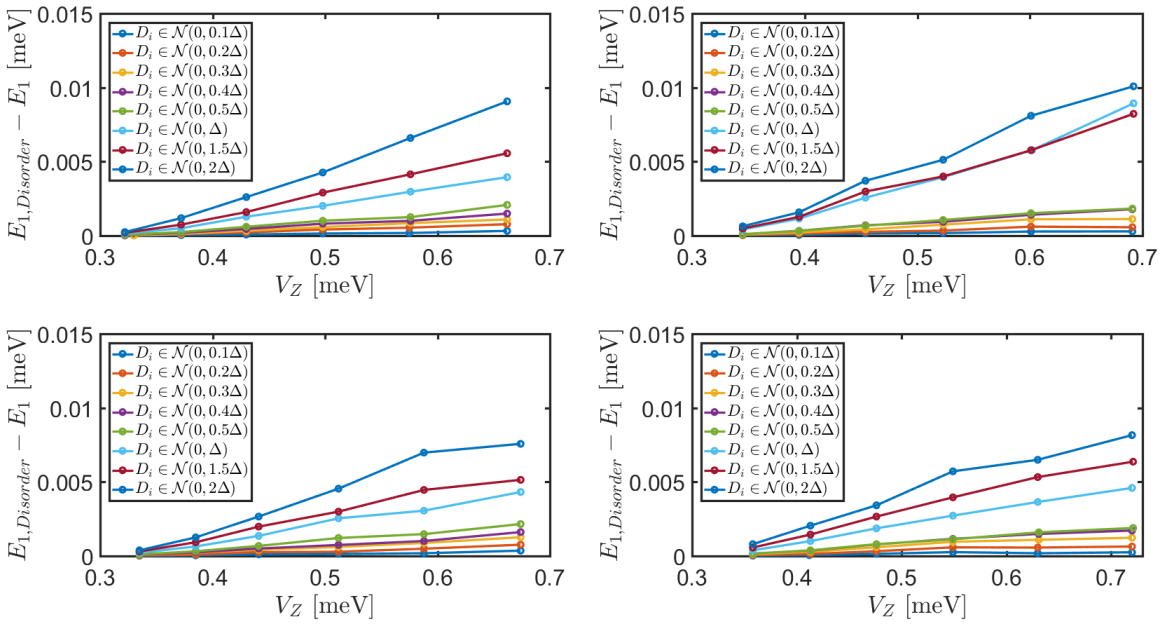

FIG. 3.24. (Top left panel) $E_{1,Disorder} - E_1$ at the points where the near-zero modes are degenerate for a homogeneous nanowire with disorder. The different lines correspond to different disorder strength, D_i. (Bottom left panel) $E_{1,Disorder} - E_1$ at the point where the near-zero modes are degenerate for a nanowire with a potential barrier. $w_{barrier} = 500\,\text{nm}$ and $V_0 = 0.2\,\text{meV}$. The different lines correspond to different disorder strength, D_i. (Top right panel) $E_{1,Disorder} - E_1$ at the point where the near-zero modes are degenerate for a nanowire with thirteen potential barriers. $w_{barrier} = 50\,\text{nm}$ and $V_0 = 0.05\,\text{meV}$. The different lines correspond to different disorder strength, D_i. (Bottom right panel) $E_{1,Disorder} - E_1$ at the point where the near-zero modes are degenerate for a nanowire with a superlattice. The superlattice barrier with is 5 nm, the distance between the barriers is 10 nm and $V_0 = 0.08\,\text{meV}$. The different lines correspond to different disorder strength, D_i.

3.5 Rotating magnetic field in nanowires with and without spin-orbit coupling

In the previous sections we have investigated how the overlap between the MBSs are affected by inducing a potential change in the nanowire and modulating this in different ways. One of the requirements for realising MBSs for nanowires with proximity induced s-wave superconductivity is the spin-orbit coupling. However, as discussed in [21], this requirement can be relaxed by using a helical magnetic field that rotates along the nanowire. This can e.g. be induced by having set of permanent magnets placed along the nanowire. We start with giving a theoretical solution to the problem and use this to compare the results we get by implementing the rotating magnetic field in the tight-binding Hamiltonian.

We begin with a Hamiltonian for a nanowire along an arbitrary direction, ξ, with proximity induced superconductivity and subject to a magnetic field. The BdG Hamiltonian is

$$\mathcal{H} = \left(\frac{p_\xi^2}{2m} - \mu\right)\tau_z + \frac{1}{2}g\mu_B\mathbf{B}(\xi)\cdot\boldsymbol{\sigma} + \Delta\tau_x. \tag{3.6}$$

This Hamiltonian is similar to the one we used before (Eq. (2.3)) except that we for now have chosen the arbitrary direction, ξ, and dropped the SO coupling term. Furthermore we still use the spin and particle-hole space, as described in Section 2.1, and all the consequences of this still applies. The next step is to make a rotation of the z-axis of the spin basis so it aligns with the direction of the magnetic field. This is done by performing a unitary transformation of the Hamiltonian [21]. The unitary operator is defined by

$$U = \exp[i(\phi/2)\sigma_{xy}] \tag{3.7}$$

where $\sigma_{xy} = [(\mathbf{B}\times\hat{\mathbf{z}})\cdot\boldsymbol{\sigma}]/|\mathbf{B}\times\hat{\mathbf{z}}|$ and $\cos\phi = \mathbf{B}\cdot\hat{\mathbf{z}}/|\mathbf{B}|$. The easiest way to find the transformed Hamiltonian, $\tilde{H} = U^\dagger HU$ is by letting $U^\dagger HU$ act on an arbitrary wave function $\phi(\xi)$. This results in

$$\tilde{H} = \left(\frac{p_\xi^2}{2m} - \mu\right)\tau_z + \tilde{H_R} + \tilde{H_2} + \frac{1}{2}g\mu_B\sigma_z + \Delta\tau_x. \tag{3.8}$$

The transformation gives two new terms, H_R and H_2. The first term is given by

$$\tilde{H_R} = \frac{\hbar}{mi}U^\dagger U' p_\xi\tau_z = \frac{\hbar}{m}\left(\frac{1}{2}\sigma_{xy}\frac{d\phi}{d\xi} + U^\dagger\frac{d\sigma_{xy}}{d\xi}\sin(\phi/2)\right)p_\xi\tau_z. \tag{3.9}$$

The term in the paranthesis is a term acting in spin space. The Hamiltonian describing SO coupling is (Eq. (2.3)) $H = \alpha p\sigma_x\tau_z$ and by comparing this with $\tilde{H_R}$ we see that they have the same structure. This implies that $\tilde{H_R}$ is describing SO coupling. Furthermore, if the field lines and the nanowire lies in the same plane this term can be simplified further. By taking $\hat{z}$ to be in the plane of the field this implies that $\sigma'_{xy} = 0$. The sign change of σ_{xy} when $\mathbf{B} \parallel \hat{\mathbf{z}}$ can be avoided by choosing [21]

$$U = \exp[i\phi\sigma_\perp/2] \tag{3.10}$$

where $\sigma_\perp$ is a constant matrix acting in spin space and describes the spin projection that is perpendicular to the magnetic field and the z-axis, and ϕ is continuous. This gives that H_R can be written

$$H_R = \alpha_{eff}\sigma_\perp p_\xi \tau_z \tag{3.11}$$

where the effective Rashba coefficient is defined as

$$\alpha_{eff} = \frac{\hbar}{2m}\frac{d\phi}{d\xi}. \tag{3.12}$$

The second term obtained from the transformation, $\tilde{H}_2$, is given by

$$\tilde{H}_2 = (-\hbar^2/2m)U^\dagger U'' = \frac{\hbar^2}{2m}\left[\left(\frac{\phi'}{2}\right)^2 - \frac{i}{2}\phi''\sigma_\perp\right]\tau_z. \tag{3.13}$$

The first term acts as a renormalization of the chemical potential. The second term has the same form as an imaginary magnetic field that is parallel to the plane of the spin orbit field. By writing this term in a symmetrized form , $(\alpha_{eff}p_\xi + p_\xi\alpha_{eff})/2$, it can be included in Eq. (3.12). Now, for this Hamiltonian to resemble the the Hamiltonian for the nanowire with SO coupling as studied in previous sections the SO coupling is required to be perpendicular to the magnetic field. To induce SO coupling with the same strength as the Rashba parameter, the derivative of the rotating magnetic field, ϕ', should be large. An optimal field for this is proposed in [21] and is given by

$$\mathbf{B}(\xi) = B_0[\sin(\xi/R), 0, \cos(\xi/R)]. \tag{3.14}$$

If we now consider the same setup as before with a nanowire in the x-direction (Section 2.1) and remembering that $\cos\phi = \mathbf{B}\cdot\hat{\mathbf{z}}/|\mathbf{B}|$ the Hamiltonian reduces to

$$\tilde{H} = \left(\frac{p^2}{2m} - \mu + \frac{\hbar^2}{8mR^2}\right)\tau_z + \alpha_{eff}p\sigma_x\tau_z + \frac{1}{2}g\mu_B B_0\sigma_z + \Delta(x) \tag{3.15}$$

where $\alpha_{eff} = \frac{\hbar}{2mR}$. Thus it is shown that an effective SO coupling can be induced in a nanowire without SO-coupling. To implement a helical magnetic field in the tight-binding model described in Section 2.2 we simply just have to consider the Zeeman term with $\boldsymbol{\sigma} = (\sigma_x, 0, \sigma_z)$. By choosing $R = 159\,\text{nm}$ this ensure that magnetic field can rotate an integer number of periods along the nanowire. Furthermore, it gives $\alpha_{eff} = \alpha_R = 9.59\cdot 10^{-12}\,\text{eVm}$, which however is a bit larger than the Rashba coefficient for InAs. In Fig. 3.25a $\{E_n\}$ as a function of V_Z is plotted. By comparison to Fig. 3.1a it is seen that the results are similar. Since the SO coupling is stronger the oscillations in the near-zero modes has been shifted slightly towards the left. This implies that the region where the splitting between the zero modes is small has become larger. The weight of the MBSs for a nanowire without SO coupling and subject to a rotating magnetic field and the weight of the MBS for a nanowire with SO coupling and with a constant magnetic field are plotted in Figs. 3.25b and 3.25c respectively. A small difference can be seen between the plots. However, by investigation this is not due to the renormalization of the chemical potential. This small difference is therefore most probably due to small differences produced by

the tight-binding description of the Hamiltonian and could possibly be reduced by increasing the number of lattice sites.

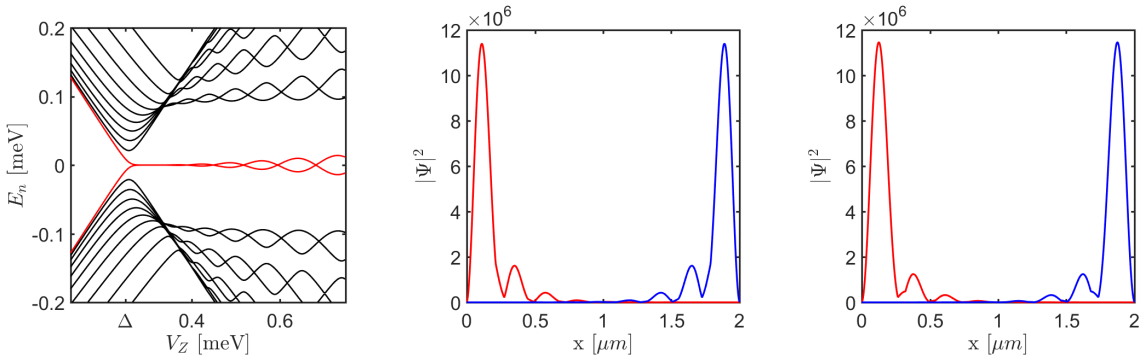

(a) (b) (c)

FIG. 3.25. (a) $\{E_n\}$ as function of V_Z for a nanowire without SO coupling and subject to a rotating magnetic field. R = 159 nm. (b) Probability density of MBSs for a nanowire without SO coupling and subject to a rotating magnetic field, R = 159 nm and $V_Z = 0.431$ meV (c) MBSs for a nanowire with SO coupling, $\alpha_R = 9.59 \cdot 10^{-12}$ and $V_Z = 0.431$ meV

The result from the case when the magnetic field is not allowed to make an integer number of rotations over the nanowire is seen in Fig. 3.26. For this $R = 190$ nm. Due to that the number of rotations is a non integer this results in two MBSs that are asymmetric and the weight of one of the MBSs is shifted towards the middle. The shift is, however, mostly to the second peak and is in this case not changing the overlap.

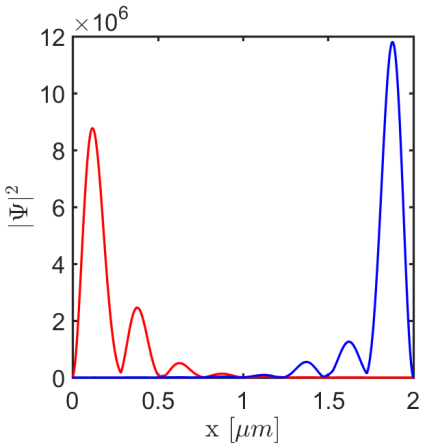

FIG. 3.26. Probability density of MBSs for a magnetic field making a non integer number of rotations over the nanowire. R = 190 nm

Now we consider a nanowire with SO coupling subject to a rotating magnetic field and as in Eq. (3.6) we add the term

$$H_\alpha = \alpha p_\xi \sigma_x \tau_z, \tag{3.16}$$

which corresponds to the SO coupling. By making the same unitary transformation Eq. (3.10) this results in

$$\tilde{H}_\alpha = \alpha p_\xi \sigma_x \tau_z + \frac{\hbar\alpha}{2R}\tau_z. \tag{3.17}$$

The first term is still the same as before the transformation, however, due to the transformation a second term has been added which corresponds to a second renormalization of the chemical potential. The total transformed Hamiltonian is then written, for a nanowire in the x-direction

$$\tilde{H} = \left(\frac{p^2}{2m} - \mu + \frac{\hbar^2}{8mR^2} + \frac{\hbar\alpha}{2R}\right)\tau_z + (\alpha_{eff} + \alpha)p\sigma_x\tau_z + \frac{1}{2}g\mu_B B_0\sigma_z + \Delta(x). \tag{3.18}$$

The effective SO-coupling induced by the rotating field is dependent on the direction of the rotation. This is seen from that $\cos\phi = \mathbf{B}\cdot\hat{\mathbf{z}}/|\mathbf{B}|$ and $\alpha_{eff} = \frac{\hbar}{2m}\frac{d\phi}{dx}$. This term can then, depending on the direction of the rotation either amplify or reduce the already existing SO coupling due to the Rashba term. In Figs. 3.27a and 3.27b $\{E_n\}$ as function of V_Z is plotted for a nanowire with SO coupling and subjected to a rotating magnetic field. For the first case (Fig. 3.27a) the magnetic field induces an effective SO coupling that is opposite to the Rashba term and since the strength is chosen to be equal the SO terms cancel each other. Beacuse of this there is only Zeeman splitting and states changes linearly with the magnetic field and, furthermore, there are no anti-crossings since there is no longer any coupling between different spin directions. Moreover, the topologically non-trivial phase is never established and the system does not support MBSs. For the second case (Fig. 3.27b) the rotating magnetic field induces a SO coupling in the same direction as the the Rashba term and thus the total SO coupling term is amplified. Due to the increased SO coupling strength the energy splitting between the zero-modes is decreased which leads to a smaller overlap between the MBSs. The MBSs are plotted in Fig. 3.27c. As seen from this plot the MBSs localize closer to the ends of the nanowire.

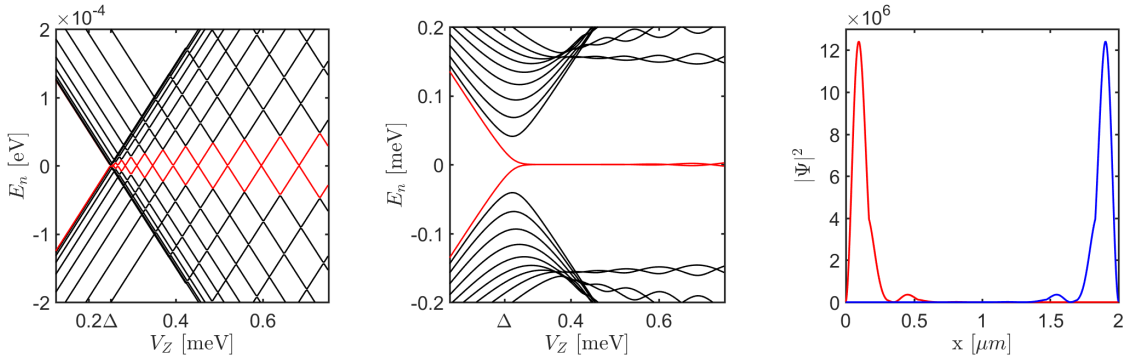

(a) (b) (c)

FIG. 3.27. (a) $\{E_n\}$ as function of V_Z for a nanowire with SO coupling and subject to a rotating magnetic field which induces an effective spin-orbit field in the opposite direction of the Rashba coupling. $R = 190\,\text{nm}$ and $\alpha_R = 8\cdot10^{-12}$. (b) $\{E_n\}$ as function of V_Z for a nanowire with SO coupling and subject to a rotating magnetic field which induces an effective spin-orbit field in the same direction of the Rashba coupling. $R = 159\,\text{nm}$ and $\alpha_R = 9.59\cdot10^{-12}$. (c) Majorana modes for a nanowire with SO-coupling and is subjected to a rotating magnetic field, $R = 159\,\text{nm}$, $\alpha_R = 9.59\cdot10^{-12}$ and $V_Z = 0.431\,\text{meV}$.

From this section we see that by using a rotating magnetic field along the wire instead of a homogeneous field we can induce SO coupling in a nanowire without SO coupling and as well control the induced coupling with the shape of the magnetic field. This also works for a nanowire with SO coupling and by using a rotating field the existing SO-coupling can both be reduced

and amplified. The induced SO coupling is, however, dependent on if it is possible to make a integer number of rotations or not. At last, by increasing the SO coupling we also see that the MBSs become more localized.

Chapter 4

Discussion

4.1 Conclusion and outlook

The aim of this thesis was to investigate if it is possible to decrease the overlap between MBSs in nanowires with spin-orbit coupling and proximity induced superconductivity by introducing different potential barriers. The problem has been addressed using a tight-binding model to describe the nanowire. For all different cases that has be investigated it is shown that the overlap between the MBSs can be made to decrease by appropriate choices of barrier parameters and Zeeman fields. The effect is, however, very small but by making further investigations it might be possible to find an optimal structure that yields the smallest overlap between the MBSs. The results also show that there are cases when the induced potential increases the overlap. This is e.g. seen for a nanowire with ten potential barriers where there is a large increase in the overlap around $V_Z \approx 0.55\,\text{meV}$. We have unfortunately not found any intuitive explanation for why the overlap is either decreasing or increasing when changing the potential structure in the nanowire. Thus this requires further studies.

Disorder in the potential has been investigated for both a homogeneous nanowire and an inhomogeneous nanowire. It has then been shown that disorder has similar effects on the inhomogeneous nanowire compared to the homogeneous nanowire for small disorder strengths. For strong disorder the homogeneous and inhomogeneous nanowire differs from each other. However, depending on the particular potential structure of the inhomogeneous nanowire the MBS overlap can be made to decrease or increase. A nanowire with one potential barrier or a superlattice is less affected by the disorder compared to the homogeneous nanowire while the nanowire with thirteen potential barriers is affected more by the disorder. Further investigations of this should include stronger disorder strengths as well as disorder in amplitude and the width of the potential barriers.

At last we follow [21] and shows that SO coupling can effectively be induced in a nanowire without SO coupling by applying a rotating magnetic field. We then extend the calculations made in [21] and show that a rotating magnetic field applied to a nanowire with SO coupling either amplifies or reduces the already existing SO coupling. It is seen that by increasing the SO coupling in the nanowire the MBSs become more localized. The rotating field that is used for this is a theoretically optimal field and may not, to the best of our knowledge, be possible to produce experimentally. Therefore one should make further investigations with a field that is more experimentally realizable. This could e.g. be a field produced by a set of permanent magnets placed next to the nanowire [21]. If this shows promising results this might be a good solution to make the MBSs more localized and the overlap between them smaller. One could

also think about combining this with a modulated potential structure to possibly achieve even better results. Further studies could also include investigation of inhomogeneous multi-mode wires to make the model more realistic and also disorder in the other parameters of the system.

Bibliography

[1] Frank Wilczek. Majorana returns. *Nat Phys*, 5(9):614–618, Sep 2009.

[2] Martin Leijnse and Karsten Flensberg. Introduction to topological superconductivity and majorana fermions. *Semiconductor Science and Technology*, 27(12):124003, 2012.

[3] T D Stanescu and S Tewari. Majorana fermions in semiconductor nanowires: fundamentals, modeling, and experiment. *Journal of Physics: Condensed Matter*, 25(23):233201, 2013.

[4] Jin-Peng Xu, Canhua Liu, Mei-Xiao Wang, Jianfeng Ge, Zhi-Long Liu, Xiaojun Yang, Yan Chen, Ying Liu, Zhu-An Xu, Chun-Lei Gao, Dong Qian, Fu-Chun Zhang, and Jin-Feng Jia. Artificial topological superconductor by the proximity effect. *Phys. Rev. Lett.*, 112:217001, May 2014.

[5] Annica M. Black-Schaffer and Jacob Linder. Majorana fermions in spin-orbit-coupled ferromagnetic josephson junctions. *Phys. Rev. B*, 84:180509, Nov 2011.

[6] Jason Alicea. New directions in the pursuit of majorana fermions in solid state systems. *Reports on Progress in Physics*, 75(7):076501, 2012.

[7] Chetan Nayak, Steven H Simon, Ady Stern, Michael Freedman, and Sankar Das Sarma. Non-abelian anyons and topological quantum computation. *Reviews of Modern Physics*, 80(3):1083, 2008.

[8] Maissam Barkeshli and Jay D. Sau. Physical architecture for a universal topological quantum computer based on a network of majorana nanowires, 2015. arXiv:1509.07135.

[9] Michael Tinkham. *Introduction to Superconductivity*. McGraw-Hill, Inc., 1996.

[10] H. Ibach and H. Lüth. *Solid-State Physics*. Springer Berlin Heidelberg, 2009.

[11] Henrik Bruus and Karsten Flensberg. *Many-Body Quantum Theory in Condensed Matter Physics*. Oxford University Press, 2004.

[12] Masatoshi Sato and Yoichi Ando. Topological superconductors. 2016. arXiv:1608.03395.

[13] David J. Griffiths. *Introduction to Electrodynamics*. Pearson, 2013.

[14] J. J. Sakurai and Jim. J Napolitano. *Modern Quantum Mechanics*. Pearson, 2013.

[15] Falko Pientka Felix von Oppen, Yany Peng. Topological superconducting phases in one dimension. `http://topo-houches.pks.mpg.de/wp-content/uploads/2015/09/lecture_Oppen.pdf` [Accessed: 2016-10-31].

[16] A. Manchon, H. C. Koo, J. Nitta, S. M. Frolov, and R. A. Duine. New perspectives for rashba spin-orbit coupling. *Nat Mater*, 14(9):871–882, Sep 2015.

[17] G. Dresselhaus. Spin-orbit coupling effects in zinc blende structures. *Phys. Rev.*, 100:580–586, Oct 1955.

[18] C. Fasth, A. Fuhrer, L. Samuelson, Vitaly N. Golovach, and Daniel Loss. Direct measurement of the spin-orbit interaction in a two-electron InAs nanowire quantum dot. *Phys. Rev. Lett.*, 98:266801, June 2007.

[19] A Yu Kitaev. Unpaired majorana fermions in quantum wires. *Physics-Uspekhi*, 44(10S):131, 2001.

[20] Yuval Oreg, Gil Refael, and Felix von Oppen. Helical liquids and majorana bound states in quantum wires. *Phys. Rev. Lett.*, 105:177002, Oct 2010.

[21] Morten Kjaergaard, Konrad Wölms, and Karsten Flensberg. Majorana fermions in superconducting nanowires without spin-orbit coupling. *Phys. Rev. B*, 85:020503, Jan 2012.

[22] F. Domínguez, J. Cayao, P. San-Jose, R. Aguado, A. Levy Yeyati, and E. Prada. Zero-energy pinning from interactions in Majorana nanowires. September 2016. arXiv:1609.01546.

[23] S. M. Albrecht, A. P. Higginbotham, M. Madsen, F. Kuemmeth, T. S. Jespersen, J. Nygård, P. Krogstrup, and C. M. Marcus. Exponential protection of zero modes in majorana islands. *Nature*, 531(7593):206–209, Mar 2016. Letter.

[24] J.H Davies. *The Physics of low-dimensional semiconductors, an introduction.* Cambridge University Press, 1998.

[25] S. Das Sarma, Jay D. Sau, and Tudor D. Stanescu. Splitting of the zero-bias conductance peak as smoking gun evidence for the existence of the majorana mode in a superconductor-semiconductor nanowire. *Phys. Rev. B*, 86:220506, Dec 2012.